NRC Research Press

ARTICLE

Understanding historical summer flounder (*Paralichthys dentatus*) abundance patterns through the incorporation of oceanography-dependent vital rates in Bayesian hierarchical models

Cecilia A. O'Leary, Timothy J. Miller, James T. Thorson, and Janet A. Nye

Abstract: Climate can impact fish population dynamics through changes in productivity and shifts in distribution, and both responses have been observed for many fish species. However, few studies have incorporated climate into population dynamics or stock assessment models. This study aimed to uncover how past variations in population vital rates and fishing pressure account for observed abundance variation in summer flounder (*Paralichthys dentatus*). The influences of the Gulf Stream Index, an index of climate variability in the Northwest Atlantic, on abundance were explored through natural mortality and stock–recruitment relationships in age-structured hierarchical Bayesian models. Posterior predictive loss and deviance information criterion indicated that out of tested models, the best estimates of summer flounder abundances resulted from the climate-dependent natural mortality model that included log-quadratic responses to the Gulf Stream Index. This climate-linked population model demonstrates the role of climate responses in observed abundance patterns and emphasizes the complexities of environmental effects on populations beyond simple correlations. This approach highlights the importance of modeling the combined effect of fishing and climate simultaneously to understand population dynamics.

Résumé : Le climat peut avoir un impact sur la dynamique des populations de poissons par le biais de modifications de la productivité et de la répartition, ces deux types de réactions ayant été observés pour de nombreuses espèces de poissons. Peu d'études ont toutefois intégré le climat à des modèles de dynamique des populations ou d'évaluation des stocks. La présente étude avait pour objectif de déterminer l'incidence de variations passées d'indices vitaux de populations et de la pression de la pêche sur les variations observées de l'abondance de cardeaux d'été (*Paralichthys dentatus*). Les influences de l'indice du Gulf Stream, un indice de variabilité du climat dans le nord-ouest de l'océan Atlantique, sur cette abondance ont été examinées par l'entremise de relations entre la mortalité naturelle et le recrutement au stock dans des modèles bayésiens hiérarchiques structurés par âge. La perte prédite a posteriori et le critère d'information associé à la somme des carrés des écarts indiquent que, des modèles mis à l'essai, les meilleures estimations des abondances des cardeaux d'été sont obtenues du modèle de mortalité naturelle dépendant du climat qui intègre des réactions log-quadratiques à l'indice du Gulf Stream. Ce modèle de population relié au climat démontre le rôle des réactions au climat dans les motifs d'abondance observés et souligne la complexité des effets environnementaux sur les populations au-delà de corrélations simples. L'approche fait ressortir l'importance de modéliser simultanément l'effet combiné de la pêche et du climat pour comprendre la dynamique des populations. [Traduit par la Rédaction]

Introduction

Water temperatures are increasing globally (Lozier et al. 2008; Belkin 2009; Hansen et al. 2010; GISTEMP Team 2018) and global climate models indicate that this warming is likely to continue (IPCC 2013). Many recent studies demonstrate that to understand factors influencing changes in fish productivity, the environment cannot be ignored (Vert-pre et al. 2013; Essington et al. 2015; Szuwalski et al. 2015). Managers utilize the productivity of a stock to set management goals, and so the effect of temperature and other environmental influences on fish stock productivity is important to management agencies. However, both climate and fishing pressure can result in shifts in productivity (Planque et al. 2010; Bell et al. 2015; Simpson et al. 2011), and so teasing apart the relative impact of fishing and climate on species' abundance is difficult (Thorson et al. 2017). Incorporating environmental drivers into fish assessment models and distinguishing fishing pressure from environmental pressure on fish stocks remain elusive.

Statistical population models can help disentangle the effects of various drivers on fish dynamics, including fishing and climate, because the models connect assumptions regarding population productivity and stability to the species' life history and its demographic rates. For example, Hare et al. (2010) suggested that the Atlantic croaker population will shift poleward as temperatures increase but will shift much less than when heavily fished. Climate can impact fish population dynamics (e.g., natural mortality and stock–recruitment) directly through physiological effects (Buckley et al. 2004; Baudron et al. 2011, 2014) or indirectly through predator–prey interactions or behaviorally mediated pro-

Received 9 March 2018. Accepted 23 September 2018.

C.A. O'Leary and J.A. Nye. School of Marine and Atmospheric Sciences, Stony Brook University, Stony Brook, NY 11794, USA.
T.J. Miller. Northeast Fisheries Science Center, National Marine Fisheries Service, 166 Water Street, Woods Hole, MA 02543, USA.
J.T. Thorson. Fisheries Resources Assessment and Monitoring Division, Northwest Fisheries Science Center, National Marine Fisheries Service, NOAA, Seattle, WA 98112, USA.
Corresponding author: Cecilia A. O'Leary (email: caoleary@uw.edu).

cesses (Blanchard et al. 2005; Laurel et al. 2007). Direct effects include physiological responses to changes in habitat differing from optimal temperature conditions (resulting in changes in the allocation of energy between growth and reproduction). Indirect effects occur through changes in community composition via the death or movement of an organism's predators or prey (Parmesan 2006). Environmental effects can alter recruitment patterns by modifying the reproductive potential of fish (Van Der Kraak and Pankhurst 1996), the timing of spawning and (or) migration (Kjesbu 1994), and larval growth (Solberg and Tilseth 1987). Studies observed environmental effects on recruitment for cod (*Gadus morhua*) and southern New England yellowtail flounder (*Limanda ferruginea*). Cod recruitment variation was linked to variations in ocean temperatures driven by North Atlantic oscillation variations off Labrador, Newfoundland, and in the Barents Sea (Mann and Drinkwater 1994; Ottersen et al. 2001; Ottersen and Stenseth 2001). For southern New England yellowtail flounder, recruitment was linked to variations in the mid-Atlantic cold pool and Gulf Stream position (Miller et al. 2016; Xu et al. 2018). Multiple other studies found that fish population fluctuations are associated with climate variations (Lehodey et al. 2006; Brander 2007, 2010; Holsman et al. 2012; Barange et al. 2014). Representations of vital rates in a climate-dependent fashion can be used to predict the consequences of different vital rate climate dependency assumptions on a fish population's status and to help separate the climate effects from fishing mortality.

To demonstrate the utility of using climate-dependent vital rates to help us (*i*) to understand how climate influenced fish in the past and (*ii*) to separate out climate effects from fishing effects, we need a fish species that was exposed to contrasting patterns in warming ocean temperature and changes in fishing pressure. One such fish is summer flounder (*Paralichthys dentatus*) whose abundance and distribution has fluctuated over the last 40 years under different fishing pressure and climate regimes. There is no consensus about the relative influence of stock recovery, fishing, or climate on these shifts (Nye et al. 2009; Pinsky et al. 2013; Bell et al. 2015). The fishing mortality rate for fully recruited (age 4) summer flounder is estimated to have declined from values greater than 1.0 in the 1980s to values below 0.5 since 2001 (Terceiro 2013, 2016). There are at least three potential explanations for summer flounder's abundance increase: (*i*) rebuilding of the stock following decreasing fishing pressure (Bell et al. 2015; Thorson et al. 2016); (*ii*) continually enhanced ocean warming in the Northwest Atlantic providing summer flounder, a warm water species, with more ideal thermal conditions and (or) more available thermal habitat (Kleisner et al. 2017); or (*iii*) a combination of favorable climate and release from fishing pressure, as there are often interactions between these two stressors (Planque et al. 2010; Fuller et al. 2015). While several studies have documented summer flounder population shifts in distribution and abundance (Nye et al. 2009; Pinsky et al. 2013; Bell et al. 2015), none provide a mechanistic understanding of the population-level processes that lead to changes and thus to differences in productivity over time.

Environmental conditions on the Northwest Atlantic Shelf, including temperature, salinity, and chlorophyll, are partially dependent on the relative strength between the cold Labrador Slope water coming from upstream and warm slope water originating from lower latitudes (Taylor et al. 1957; Townsend et al. 2010; Mountain 2012; Greene et al. 2013; Xu et al. 2015). The best leading indicator of this coupled slope water process is the position of the north wall of the Gulf Stream (Nye et al. 2011; Saba et al. 2016). While there are individual environmental covariates that co-occur with shifts in the Gulf Stream position, the position of the north wall of the Gulf Stream at depth, hereafter referred to as the Gulf Stream Index (GSI), captures many of these changes in a single index (Joyce et al. 2000; Peña-Molino and Joyce 2008). The correlation between the GSI and seasonal mean stratified bottom temperature over the entire shelf was noted in Nye et al. (2011) at $r = 0.51$ (lag = 0). The GSI also indicates the volume of the mid-Atlantic cold pool and consequently reduced stratification (Xu et al. 2018). Thus, we selected this large-scale indicator to investigate the effects of environmental conditions on fish population dynamics (Hallett et al. 2004).

This paper has two aims: (*i*) to determine if the incorporation of environmental covariates can improve population parameter estimates using the GSI as a proof of concept and (*ii*) to investigate the influence of climate and fishing on summer flounder abundance over time by evaluating the GSI impact on natural mortality and recruitment in a Bayesian hierarchical model framework. We hypothesized that models with some form of climate dependency in both natural mortality and recruitment alongside varying fishing mortality would best estimate past summer flounder abundances. We used a spatially aggregated model to represent dynamics across the stock's range and included a climate-dependent relationship for recruitment and (or) natural mortality to account for both direct and indirect mechanisms.

Methods

This paper investigated the influence of both climate and fishing on summer flounder abundance and demonstrated the use of statistical models to incorporate environmental influences on population vital rates. Overall, we developed an age-structured hierarchical population model with time-varying fishing mortality. This model was then adjusted to test various hypotheses regarding the influence of climate on recruitment and natural mortality. A total of 20 models were created, each parameterizing natural mortality, recruitment, or both, in a climate-dependent fashion to determine what combination of climate dependency and fishing mortality best estimates past summer flounder abundances.

Models

We used age-structured hierarchical models that treated the population as a single stock with observation error in both the catch-at-age ($C_{a,t}$) and index-at-age ($I_{a,t}$) terms and process error in both recruitment and natural mortality (eqs. 3–7; King 2012; Terceiro 2013, 2016).

Equations 1 and 2 below describe the general population process model. Summer flounder abundance ($N_{a,t}$) was estimated across time (t) by age (a) from age-at-recruitment ($a = 0$) to age 7+ (any fish age 7 or older was treated as a "plus group") (eqs. 1*a*, 1*b*), consistent with the stock assessment (Terceiro 2013, 2016), where abundance was affected by recruitment R_t for each year t and survival ($e^{-Z_{a,t}}$) for each year and age:

$$(1a)\qquad N_{a,t} = \begin{cases} R_t & a = 0 \\ e^{-Z_{a-1,t-1}} N_{a-1,t-1} & 1 \le a \le 6 \\ e^{-Z_{a-1,t-1}} N_{a-1,t-1} + e^{-Z_{a,t-1}} N_{a,t-1} & a \ge 7 \end{cases}$$

$$(1b)\qquad R_t \sim \mathrm{LN}\left[\log\left(\frac{\alpha B_{t-1}}{1 + \beta_2 B_{t-1}}\right), \lambda_R\right]$$

Log-abundance ($\log(N_{a,t=0})$) in the first modeled year was assigned a uniform prior distribution with realistic biological bounds selected such that the posterior distribution did not approach its values and affect model results. Total mortality was $Z_{a,t} = M_{a,t} + F_{a,t}$. Natural mortality ($M_{a,t}$) and fishing mortality rates ($F_{a,t}$) varied across time and age classes. Fishing mortality occurred from age class 0 and up, based on stock assessment reports of fishing pressure (Terceiro 2013, 2016). Fishing was parameterized with separable age and year components with an associated selectivity-at-age and fully selected annual fishing mortality rate. Natural mortality ($M_{a,t}$) was modeled in all forms presented in the following sections as a stochastic process, with values drawn from

a lognormal distribution with mean ($V_{a,t}$; hyperparameter for log-natural mortality) and precision (λ_M; the inverse of the variance). The climate-independent form of the natural mortality was $M_{a,t} \sim \text{LN}(V_{a,t}, \lambda_M)$, where $V_{a,t} = \beta_0$ (Table 1).

Recruitment (R_t) or abundance at $a = 0$ was lognormally distributed with a mean Beverton–Holt function of the spawning stock biomass (B_{t-1}) from the previous year ($t - 1$), alpha (α), and beta (β_2) as modeled in the stock assessment (eq. 1*b*; Terceiro 2013, 2016). The variability of recruitment was parameterized with precision parameter λ_R (the inverse of the variance).

Per the stock assessment, 90% of age class 1 and 99% of age class 2 were reported as mature, and so the appropriate coefficients were included in the spawning stock biomass equation (Terceiro 2013, 2016; eq. 2). The $w_{a,t}$ variables represent the weight-at-age for $a = 1, \ldots, 7+$, and here we assumed that weight-at-age varies temporally (M. Terceiro, NEFSC, Massachusetts, personal communication). A 50:50 ratio of males to females was assumed (a slightly different assumption than in the stock assessment; Terceiro 2016), and so half of the remaining fish from age classes 1 to 7+ contributed to spawning stock biomass. Spawning stock biomass (B_t) was dependent upon the abundance at age a at time t ($N_{a,t}$), empirical weight at age a at time t ($w_{a,t}$), and the proportion mature at age a (p_a) up to the final age class A.

$$B_t = \frac{1}{2}\sum_{2}^{A} N_{a,t} w_{a,t} p_a \quad (2)$$

The expected index at age a at time t ($I_{a,t}$) was a function of catchability (q), selectivity at age a and block b ($S_{a,b}$), total mortality ($Z_{a,t}$), and the fraction of the year elapsed when data were collected (π set to 1 year) as $I_{a,t} = q_t S_{a,b} e^{-Z_{a,t},\pi} N_{a,t}$. Catchability ($q_t$) for the fisheries-independent data was annually time-varying and estimated within the model for each year. Selectivity for the fisheries-independent data was separated into two time-period blocks and assumed to be age-dependent. The two blocks were from 1982 to 1995 and 1996 to 2015, similar to the stock assessment, and specified to correspond to the implementation of commercial management regulation change in 1996 (Terceiro 2013, 2016). Selectivity at age a and block b ($S_{a,b}$) was estimated as time-constant within those blocks. Catch ($C_{a,t}$) was a function of natural ($M_{a,t}$) and fishing ($F_{a,t}$) mortality at age a at time t, using the Baranov catch equation and assuming that fishing was continuous throughout the year $C_{a,t} = \frac{F_{a,t}}{F_{a,t}+M_{a,t}}[1 - e^{-(M_{a,t}+F_{a,t})}]N_{a,t}$. The general observation model included both indices-at-age data ($I^*_{a,t}$) and catch-at-age data ($C^*_{a,t}$) that were lognormally distributed with assumed known precision for the index (λ_N) and for the catch (from discard and recreational landing data) (λ_c) as $I^*_{a,t} \sim \text{LN}[\log(I_{a,t}), \lambda_N]$ and $C^*_{a,t} \sim \text{LN}[\log(C_{a,t}), \lambda_c]$.

The null model included all climate-independent parameters. We tested a total of 20 models (Table 1). Tested models included all forms of natural mortality and recruitment scenarios and their interactions (see https://github.com/ceciliaOLearySBU/Bayesian_hierarchical_GSI_model). The following sections describe each of the climate-dependent recruitment and natural mortality options that were tested both in isolation and in all possible pairwise comparisons.

Recruitment climate dependency forms

The climate-independent recruitment model took a standard Beverton–Holt form as in eq. 1*b*. Multiple climate-dependent forms of recruitment were evaluated as alternative assumptions. The climate-dependent recruitment models used the climate responses explored in Fry (1971) and expanded upon by Neill et al. (1994) and Iles and Beverton (1998) to integrate climate-dependent recruitment at time t (R_t) in three different functional forms: controlling (eq. 3), limiting (eq. 4), and masking (eq. 5). Here, c was a scalar factor for the effect of an environmental index on recruitment, and T_t was an environmental factor, in this case, the GSI. In all three equations (3–5), λ_R was the precision for the recruitment term, or the inverse of the variance.

$$R_t = \text{LN}\left[\log\left(\frac{B_{t-1}e^{cT_t}}{\beta_2 + \alpha B_{t-1}}\right), \lambda_R\right] \quad (3)$$

$$R_t = \text{LN}\left[\log\left(\frac{B_{t-1}}{\beta_2 + \alpha e^{cT_t} B_{t-1}}\right), \lambda_R\right] \quad (4)$$

$$R_t = \text{LN}\left[\log\left(\frac{B_{t-1}}{\beta_2 e^{cT_t} + \alpha B_{t-1}}\right), \lambda_R\right] \quad (5)$$

Controlling factors generally impact the metabolic rate by placing bounds on the chemical reactions. Limiting factors generally restrict the supply of materials in the metabolic chain, and masking factors influence how energy is channeled in an organism (Fry 1971; Morse 1981; Iles and Beverton 1998). For each recruitment climate-dependent assumption tested, one of these equations replaced eq. 1*b* in the model (see Table 1 for each model equation details). Each of these climate-dependent forms was paired with either climate-independent or climate-dependent natural mortality.

Natural mortality climate dependency forms

Multiple climate-dependent forms of natural mortality were evaluated as alternative assumptions. Natural mortality was parameterized as a log-linear function of GSI (T_t; represents either the GSI value for the log-linear climate dependency or a linear transformation for the log-quadratic climate dependency) with slope (β_1), intercept (β_0), and a quadratic effect (β_2) (eqs. 6, 7). Four relationships were tested between GSI and natural mortality including (*i*) log-quadratic (eq. 6), (*ii*) log-linear (eq. 6, where $\beta_2 = 0$), (*iii*) log-quadratic by age (eq. 7), and (*iv*) log-linear by age (eq. 7, where $\beta_{2,a} = 0$) using variations of the two equations below.

$$V_{a,t} = \beta_0 + \beta_1 T_t + \beta_2 T_t^2 \quad (6)$$

$$V_{a,t} = \beta_{0,a} + \beta_{1,a} T_t + \beta_{2,a} T_t^2 \quad (7)$$

For each natural mortality climate-dependent assumption tested, one of these equations replaced $V_{a,t} = \beta_0$ in the model (see Table 1 for each model equation details). The climate-dependent or climate-independent natural mortality value was then incorporated into the survival equation. The log-quadratic form was configured orthogonally with the poly() function in R (eqs. 6, 7). In other words, T_t is the monic orthogonal polynomial of GSI for the log-quadratic functional forms. A log-linear response of natural mortality to GSI is based on the hypothesis that natural mortality increases linearly with GSI. A nonlinear response of natural mortality to GSI is based on the concept that there is an optimal environmental condition above and below which natural mortality increases.

Scenarios

The above-described climate dependencies for both natural mortality and recruitment were tested concurrently with time-varying fishing mortality to understand their relative role in estimating past summer flounder abundances. First, a baseline model that is completely climate-independent (TI) was introduced to serve as a null hypothesis (Table 1). Then, a total of four models tested climate-dependent natural mortality in isolation from all other climate dependencies: log-linear (LM), log-quadratic (QM), age-dependent log-linear (AM), and age-dependent log-quadratic

Table 1. Models tested with varying forms of climate dependency, where $M_{a,t} \sim \text{LN}(V_{a,t}, \lambda_M)$ and natural mortality models differ by their parameterization for $V_{a,t}$, the mean value for the lognormal distribution of natural mortality ($M_{a,t}$).

Model description (abbreviation)	$V_{a,t}$ parameterization	E[log(R_t)] parameterization	No. of estimated parameters	Time (t) and age (a) varying parameters
1. Climate-independent (TI)	β_0	$\frac{\alpha S_{t-1}}{1+\beta_2 S_{t-1}}$	584	$F(a,t)$, $M(a,t)$, $q(t)$
2. Log-linear climate-dependent natural mortality (LM)	$\beta_0 + \beta_1 T_t$	$\frac{\alpha S_{t-1}}{1+\beta_2 S_{t-1}}$	586	$F(a,t)$, $M(a,t)$, $q(t)$
3. Log-quadratic climate-dependent natural mortality (QM)	$\beta_0 + \beta_1 T_t + \beta_2 T_t^2$	$\frac{\alpha S_{t-1}}{1+\beta_2 S_{t-1}}$	587	$F(a,t)$, $M(a,t)$, $q(t)$
4. Age-dependent log-linear climate-dependent natural mortality (AM)	$\beta_{0,}a + \beta_{1,a} T_t$	$\frac{\alpha S_{t-1}}{1+\beta_2 S_{t-1}}$	600	$F(a,t)$, $M(a,t)$, $q(t)$, $\beta_0(a)$, $\beta_1(a)$
5. Age-dependent log-quadratic climate-dependent natural mortality (NQA)	$\beta_{0,a} + \beta_{1,a} T_t + \beta_{2,a} T_t^2$	$\frac{\alpha S_{t-1}}{1+\beta_2 S_{t-1}}$	608	$F(a,t)$, $M(a,t)$, $q(t)$, $\beta_0(a)$, $\beta_1(a)$, $\beta_2(a)$
6. Controlling recruitment (CR)	β_0	$\frac{S_{t-1} e^{cT}}{\beta_2 + \alpha S_{t-1}}$	585	$F(a,t)$, $M(a,t)$, $q(t)$
7. Limiting recruitment (LR)	β_0	$\frac{S_{t-1}}{\beta_2 + \alpha e^{cT} S_{t-1}}$	585	$F(a,t)$, $M(a,t)$, $q(t)$
8. Masking recruitment (MR)	β_0	$\frac{S_{t-1}}{\beta_2 e^{cT} + \alpha S_{t-1}}$	585	$F(a,t)$, $M(a,t)$, $q(t)$
9. Log-linear climate-dependent natural mortality + controlling recruitment (LMCR)	$\beta_0 + \beta_1 T_t$	$\frac{S_{t-1} e^{cT}}{\beta_2 + \alpha S_{t-1}}$	587	$F(a,t)$, $M(a,t)$, $q(t)$
10. Log-linear climate-dependent natural mortality + limiting recruitment (LMLR)	$\beta_0 + \beta_1 T_t$	$\frac{S_{t-1}}{\beta_2 + \alpha e^{cT} S_{t-1}}$	587	$F(a,t)$, $M(a,t)$, $q(t)$
11. Log-linear climate-dependent natural mortality + masking recruitment (LMMR)	$\beta_0 + \beta_1 T_t$	$\frac{S_{t-1}}{\beta_2 e^{cT} + \alpha S_{t-1}}$	587	$F(a,t)$, $M(a,t)$, $q(t)$
12. Log-quadratic climate-dependent natural mortality + controlling recruitment (QMCR)	$\beta_0 + \beta_1 T_t + \beta_2 T_t^2$	$\frac{S_{t-1} e^{cT}}{\beta_2 + \alpha S_{t-1}}$	588	$F(a,t)$, $M(a,t)$, $q(t)$
13. Log-quadratic climate-dependent natural mortality + limiting recruitment (QMLR)	$\beta_0 + \beta_1 T_t + \beta_2 T_t^2$	$\frac{S_{t-1}}{\beta_2 + \alpha e^{cT} S_{t-1}}$	588	$F(a,t)$, $M(a,t)$, $q(t)$
14. Log-quadratic climate-dependent natural mortality + masking recruitment (QMMR)	$\beta_0 + \beta_1 T_t + \beta_2 T_t^2$	$\frac{S_{t-1}}{\beta_2 e^{cT} + \alpha S_{t-1}}$	588	$F(a,t)$, $M(a,t)$, $q(t)$
15. Age-dependent log-linear climate-dependent natural mortality + controlling recruitment (AMCR)	$\beta_{0,a} + \beta_{1,a} T_t$	$\frac{S_{t-1} e^{cT}}{\beta_2 + \alpha S_{t-1}}$	601	$F(a,t)$, $M(a,t)$, $q(t)$, $\beta_0(a)$, $\beta_1(a)$
16. Age-dependent log-linear climate-dependent natural mortality + limiting recruitment (AMLR)	$\beta_{0,a} + \beta_{1,a} T_t$	$\frac{S_{t-1}}{\beta_2 + \alpha e^{cT} S_{t-1}}$	601	$F(a,t)$, $M(a,t)$, $q(t)$, $\beta_0(a)$, $\beta_1(a)$
17. Age-dependent log-linear climate-dependent natural mortality + masking recruitment (AMMR)	$\beta_{0,a} + \beta_{1,a} T_t$	$\frac{S_{t-1}}{\beta_2 e^{cT} + \alpha S_{t-1}}$	601	$F(a,t)$, $M(a,t)$, $q(t)$, $\beta_0(a)$, $\beta_1(a)$
18. Age-dependent log-quadratic climate-dependent natural mortality + controlling recruitment (NQACR)	$\beta_{0,a} + \beta_{1,a} T_t + \beta_{2,a} T_t^2$	$\frac{S_{t-1} e^{cT}}{\beta_2 + \alpha S_{t-1}}$	609	$F(a,t)$, $M(a,t)$, $q(t)$, $\beta_0(a)$, $\beta_1(a)$, $\beta_2(a)$
19. Age-dependent log-quadratic climate-dependent natural mortality + limiting recruitment (NQALR)	$\beta_{0,a} + \beta_{1,a} T_t + \beta_{2,a} T_t^2$	$\frac{S_{t-1}}{\beta_2 + \alpha e^{cT} S_{t-1}}$	609	$F(a,t)$, $M(a,t)$, $q(t)$, $\beta_0(a)$, $\beta_1(a)$, $\beta_2(a)$
20. Age-dependent log-quadratic climate-dependent natural mortality + masking recruitment (NQAMR)	$\beta_{0,a} + \beta_{1,a} T_t + \beta_{2,a} T_t^2$	$\frac{S_{t-1}}{\beta_2 e^{cT} + \alpha S_{t-1}}$	609	$F(a,t)$, $M(a,t)$, $q(t)$, $\beta_0(a)$, $\beta_1(a)$, $\beta_2(a)$

Note: Recruitment takes the form of $R_t = \text{LN}\{\text{E}[\log(R_t)], \lambda_R\}$, and models differ by their parameterization for E[log(R_t)].

(NQA). Natural-mortality models included the linear and nonlinear forms of climate dependency both with and without age-specific forms. Next, the three climate-dependent recruitment models were tested in isolation from all other climate dependencies: controlling (CR), limiting (LR), and masking (MR). Lastly, the final 12 models test all possible pairwise comparisons of each of these natural mortality and recruitment climate-dependent forms. The names found in Table 1 for each of the final 12 models are descriptors of the two forms of climate dependency incorporated with the natural mortality form first followed by the recruitment form. The combination of four natural mortality hypotheses and three recruitment hypotheses results in the 12 total pairings of natural mortality and recruitment climate-dependent models (see Table 1 for complete notation). These scenarios aimed to estimate past abundances to understand better if the environment influenced any specific summer flounder vital rate at the same time as a temporally varying fishing mortality.

Data

We used data from both fisheries-independent and fisheries-dependent sources to inform the index and catch observation models, respectively, for the hierarchical age-structured models described in the previous sections.

Fisheries-independent data

Fisheries-independent data were collected in spring and fall annual bottom trawl surveys by the Northeast Fisheries Science Center (NEFSC) from 1968 to 2016. The surveys occur along the northeast United States continental shelf from Cape Hatteras, North Carolina, to Georges Bank and the Gulf of Maine. This survey uses a stratified random sampling design in which the number of stations sampled per stratum is proportional to its area and are randomly selected within strata (Azarovitz 1981; Clark et al. 1997). In 2009 there was a vessel change, and so a calibration was used to compare the catchability of an old vessel to a new vessel (Brown 2009; Miller 2013; M. Terceiro, NEFSC, Massachusetts, personal communication). Annual proportions-at-age were provided from previous summer flounder work that calculated proportions-at-age using the NEFSC bottom trawl survey frequency of age by length and the NEFSC bottom trawl survey proportion at length (Terceiro 2013, 2016). Mean stratified abundances, or mean catch per tow, were estimated from the counts per stratum by the area and numbers of tows per stratum and used in models.

The annual summer flounder abundance indices from the fall and spring fisheries-independent survey were pooled within each year by age, and the associated fall and spring variances were summed for the total observation error model input. This was to provide a large-scale overview of abundance patterns while avoiding the pitfalls typically associated with seasonally specific bottom trawl surveys and spawning migrations that include inshore–offshore movement in species such as summer flounder (e.g., seasonal surveys might miss fish if their inshore–offshore movement does not align with the timing of the survey or if the phenology of seasons changes, etc.; Ottersen et al. 2002). Pooling the data generated an annual summer flounder abundance signature that was consistent with the annual oceanographic signature used (see GSI explained below) and reduced the seasonal variability in the fisheries-independent data. It was assumed that the variance captured the difference in catchabilities that would exist between seasonal surveys (particularly as catchability can vary each year in the models used). The same annually varying age–length key was used for each season as in the stock assessment.

Fisheries-dependent data

Fisheries-dependent data from commercial and recreational landings of summer flounder were drawn from the NEFSC fisheries database and are available from 1982 to 2015. See Burns et al. (1983) for sampling protocols for the commercial methods. Here, we assumed that fishing operations could be approximated as homogeneous among vessels and, therefore, incorporated all fishing activity as a single fishing fleet. This decision is consistent with the description of fishing in the updated stock assessment, in which catches from the commercial and recreational fleets are combined. However, this can potentially lead to misspecification of total catch and to observation error due to potential differences in effort and catchability between fleets. Recreational catch and discards were estimated by the Marine Recreational Information Program and were combined with the landings data (Terceiro 2013, 2016). The uncertainty in the recreational catch and discard estimates provided estimates of observation error for the total catch.

Climate data

Climate data draw from the Gulf Stream Index (Fig. 1), which indicates the location of the north wall of the Gulf Stream. GSI data are available from 1954 to 2015. A positive GSI is associated with higher shelf temperatures at depth and therefore less stratified water, a stronger current system, and less cross-shelf warm core eddies (Nye et al. 2011; Andres 2016; Monim 2017), and thus serves as a proxy for both the bottom temperature and oceanographic conditions in our population models. Spring mean-stratified bottom temperatures in southern New England, the center of distribution for summer flounder, increase when the Gulf Stream shifts from a southerly position (GSI ≈ –1) to a more northerly position (GSI ≈ 2) (Fig. 1; Nye et al. 2011). The GSI was previously calculated by Lequan Chi using an empirical orthogonal function analysis of the 15 °C isotherm at 200 m depth at nine latitudes along the Gulf Stream path (Fig. 1; Joyce et al. 2000; Joyce and Zhang 2010).

We used the GSI as a basin-scale index that captures the emergent properties of the marine environment at large spatial and temporal scales, matching the scale of the summer flounder population dynamics. Xu et al. (2018) demonstrated a correlation between the GSI and yellowtail flounder recruitment, another flatfish. Preliminary analyses on a subset of the data and information criterion indicated that the GSI was a better fit in models tested than was bottom temperature. Although other indicators may better explain summer flounder population dynamics, the GSI was chosen as the environmental covariate to illustrate how climate dependency could be tested in this Bayesian framework. The detrended GSI allows us to look at the interaction of the GSI cyclical pattern and the summer flounder abundance rather than just long-term trends in the two time series (Barton et al. 2003).

Parameter estimation and priors

Information on priors for each of the model parameters was drawn from a combination of sources informing the biologically expected bounds of each parameter. Most priors, except for recruitment process error, were weakly informative or semi-informative (Table 2). Weakly informative implies that the parameter was set with a prior that limited it to reasonable biological bounds (e.g., fishing mortality is set to have equal probability for all realistic values between 0 and 2.2) but did not use any summer flounder-specific information. This lack of information was either due to a lack of available studies with summer flounder-specific information for that parameter or the available information for that parameter was from the same data source as used in the model and so was not considered. Semi-informative implies that the information was slightly more informative than just reasonable biological bounds and included flatfish-specific (but not summer-flounder-specific) information. Informative means that the information for the prior came from a summer-flounder-specific study that used data other than those used in these models. The distributions of priors defined in Table 2 were used for parameters in models defined in Table 1. Notably, the prior for the natural mortality log-mean $V_{a,t}$ limits the distribution of natural mortality ($M_{a,t}$) from 0.14 to 0.94 (Table 2). This was based upon the

Fig. 1. Spring mean stratified bottom temperature (>100 m) in southern New England (grey dotted line) from 1968 to 2009 and the detrended Gulf Stream Index (GSI; solid black line) from 1968 to 2015. The black dotted horizontal line marks zero. The analysis used GSI data from 1982 to 2015.

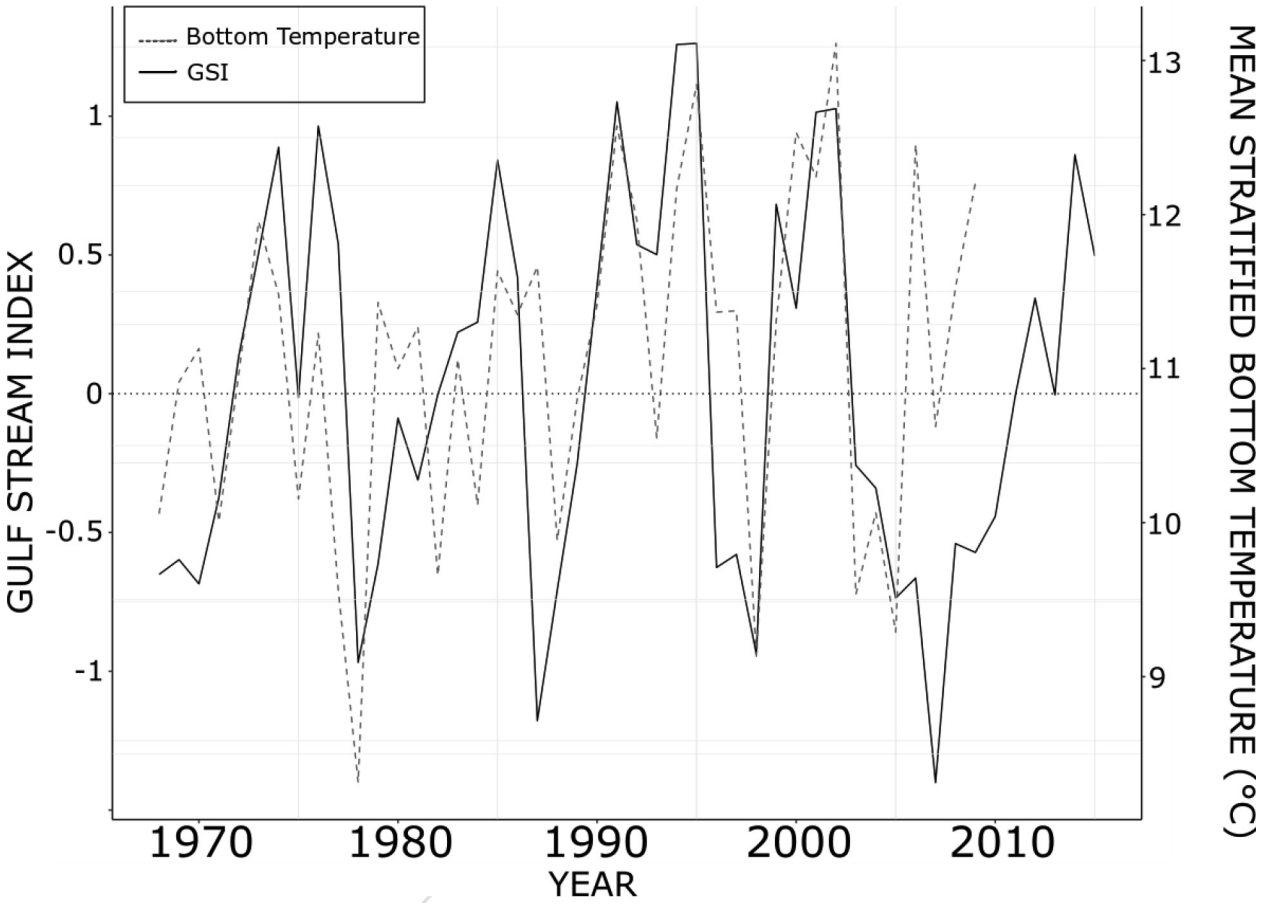

Table 2. Descriptions of parameters, parameter prior distributions, and the amount of information in each prior.

Parameter	Definition	Prior[a]	Information[b]	Mean	CV
q_t	Catchability	LN(−1.2,3)	Semi-informative	0.30	1.62
$F_{a,t}$	Fishing mortality	U(0,2.2)	Weakly informative	1.1	0.58
$S_{a,b}$	Selectivity at age a and block b	U(0,1)	Weakly informative	0.5	0.58
α	The number of recruits per spawner at low numbers of spawners in recruitment model	LN(3,1)	Weakly informative	20.09	0.03
β_2	Controls the level of density dependence in recruitment model	LN(2,1)	Weakly informative	7.39	0.08
λ_M	Natural mortality precision	U(2,10)	Uninformative	6	0.38
β_1	Natural mortality equation slope	N(0,1)	Uninformative	0	SD = 1
β_0	Natural mortality equation intercept	U(−1,1)	Semi-informative	0	SD = 0.57
λ_R	Recruitment precision	LN(−0.44,10)	Informative	0.64	0.47
$V_{a,t}$	Hyperparameter for log-mean of natural mortality	U(−1,1)	Semi-informative	0	SD = 0.57
C	Parameter scaling the effect of the incorporated environmental covariate on recruitment	N(0,0.001)	Uninformative	0	SD = 31.62

[a]LN(mean,precision), N(mean,precision), U(start,end); precision = 1/SD. For the standard normal and uniform centered on zero, the standard deviation (SD) rather than coefficient of variation (CV) was reported.

[b]Uninformative, no information; weakly informative, realistic biological bounds; semi-informative, additional bound information; informative, draws numbers from studies.

decision to both match the prior of $V_{a,t}$ to that of β_0 based upon a sensitivity analysis and the need to make similar assumptions regarding natural mortality across models. This decision also avoided prior decisions based on the stock assessment to avoid basing model assumptions upon other model assumptions. A semi-informative prior was used to inform uncorrelated annual estimation of catchability for the fisheries-independent data (Table 2; Somerton 1996; Richardson et al. 2014). This was done to prevent catchability as an explanation of temporally varying abundance when catchability was estimated as temporally static.

Bayesian parameter estimation was performed using the Just Another Gibbs Sampler (Plummer 2003) program integrated through R version 3.2.4 (R Core Team 2017) using R package R2Jags (Su and Yajima 2012). Each model had two million iterations for each of three chains to ensure convergence. A total of 50 000 samples were discarded at burn-in and a thinning rate of 1000 was

Table 3. Model selection for all 20 models presented as the sum of the change in posterior predictive loss (ΔPPL) and change in deviance information criterion (ΔDIC) from the best model (lowest value) for both the survey (N) and catch (C) observation model.

Model	ΔPPL	ΔDIC	Ranking (PPL, DIC)[a]	Average ranking[b]
Log-quadratic climate-dependent natural mortality (QM)[c]	0	3.83	(1, 2)	1.5
Age-dependent log-linear climate-dependent natural mortality (AM)	133.02	11.06	(2, 6)	4
Age-dependent log-quadratic climate-dependent natural mortality + controlling recruitment (NQACR)	927.6	9.74	(7, 4)	5.5
Age-dependent log-quadratic climate-dependent natural mortality (NQA)	631.95	11.24	(5, 7)	6
Log-quadratic climate-dependent natural mortality + controlling recruitment (QMCR)	160.81	13.98	(3, 11)	7
Log-linear climate-dependent natural mortality + limiting recruitment (LMLR)	118 015	5.32	(11, 3)	7
Age-dependent log-linear climate-dependent natural mortality + masking recruitment (AMMR)	122 169	0	(16, 1)	8.5
Log-quadratic climate-dependent natural mortality + masking recruitment (QMMR)	118 706	10.63	(13, 5)	9
Log-linear climate-dependent natural mortality (LM)	226.89	21.17	(4, 14)	9
Log-quadratic climate-dependent natural mortality + limiting recruitment (QMLR)	117 362	12.46	(10, 9)	9.5
Age-dependent log-linear climate-dependent natural mortality + controlling recruitment (AMCR)	700.04	15.01	(6, 13)	9.5
Log-linear climate-dependent natural mortality + masking recruitment (LMMR)	119 079	11.94	(14, 8)	11
Age-dependent log-linear climate-dependent natural mortality + limiting recruitment (AMLR)	1005.6	23.51	(8, 15)	11.5
Age-dependent log-quadratic climate-dependent natural mortality + limiting recruitment (NAQLR)	118 600	14.72	(12, 12)	12
Log-linear climate-dependent natural mortality + controlling recruitment (LMCR)	3 140.8	23.79	(9, 16)	12.5
Age-dependent log-quadratic climate-dependent natural mortality + masking recruitment (NQAMR)	120 153	12.95	(15, 10)	12.5
Controlling recruitment (CR)	126 142	36.08	(17, 17)	17
Climate-independent (TI)	126 258	40.03	(18, 18)	18
Masking recruitment (MR)	126 711	40.03	(20, 18)	19
Limiting recruitment (LR)	126 604	50.59	(19, 20)	19.5

[a]Ranking (PPL, DIC) ranks values lowest to highest based on PPL values first and then DIC values.
[b]Average ranking averages the PPL and DIC ranking.
[c]Best overall model out of the tested models (i.e., ranked lowest for the combination of DIC and PPL).

used, resulting in 5850 samples per posterior distribution. Model parameters were initialized by random draws from a uniform distribution with a mean centered on the mean data value. Each Markov chain ran through enough iterations to reach apparent convergence on the stationary distribution. The use of multiple chains with different starting points allowed for inspection for evidence of nonconvergence on the correct distribution.

Model selection and performance

Convergence was assessed using plots of each chain and the Gelman–Rubin shrinkage diagnostic. Model selection was based on posterior predictive loss (PPL) and deviance information criterion (DIC). PPL is an approach for scoring models based on decision theory (Hooten and Hobbs 2015) and uses the distribution function of each of the observation models to minimize the posterior loss. Output values express the log-likelihood of that parameter estimate based upon the assumed distributions and dependent on the variance (Hooten and Hobbs 2015). Differences in the PPL are interpreted the same way as differences in DIC, Akaike information criterion (AIC), and Watanabe–Akaike information criterion (WAIC) as both approaches use the log-likelihood (i.e., differences of 1–2 units deserve consideration, and DIC differences of >3 units are considerable support for the best model; Burnham and Anderson 1998). PPL was used because it applies to any Bayesian model (Gelfand and Ghosh 1998). DIC is a semi-Bayesian version of AIC to measure predictive accuracy using deviance and a correction for the effective number of parameters. WAIC was not used because it requires independent data (Gelman et al. 2014; Hooten and Hobbs 2015; Broms et al. 2016), a requirement that is not met by our temporally correlated data set. Model selection was based on both DIC and PPL. DIC and PPL each have different strengths and weaknesses and provide a different ranking of models. Therefore, in this study, the two metrics were used to rank models from best (lowest DIC and PPL value) to worst performing model. The models combined DIC and PPL and ranking was then averaged to consider model performance based on both metrics. The best performing model, therefore, has the close-to-best (i.e., lowest value) performance for both DIC and PPL combined.

PPL was calculated using the negative log-likelihood for both observation models (fisheries-dependent and fisheries-independent age composition observations) based on the lognormal distribution assumption for the indices-at-age data ($I^*_{a,t}$) and catch-at-age ($C^*_{a,t}$) data. PPL was calculated across ages a to A and years j to J as

$$\mathrm{PPL} = \frac{1}{N}\sum_{n=1}^{N}\sum_{j=1}^{J}\sum_{a=1}^{A} -\log\left[\frac{1}{x_j\sigma_n\sqrt{2\pi}}\mathrm{e}^{\frac{(\ln x_j - \mu_{n,j})^2}{2\sigma_N^2}}\right] + \frac{1}{N}\sum_{n=1}^{N}\sum_{j=1}^{J}\sum_{a=1}^{A} -\log\left[\frac{1}{y_j\sigma_n\sqrt{2\pi}}\mathrm{e}^{\frac{(\ln y_j - v_{n,j})^2}{2\sigma_N^2}}\right]$$

where n is the number of simulated data sets for a total of N = 15 000, using each of the 20 tested model frameworks. A total of 15 000 new data sets were simulated from the posterior distributions by randomly drawing from a posterior sample for each parameter from each respective model and then simulating the data given that posterior sample. The respective means for the fisheries-independent ($\mu_{n,j}$) and fisheries-dependent ($v_{n,j}$) simulated observation models for each of the n times for each year j were then used in the PPL calculation. For each model, this was then summed over the total time steps (j) in the model for a total of J = 34 time steps. The total PPL was the sum of both the fisheries-independent observations (x_j; NEFSC bottom trawl data) and the fisheries-dependent observations (y_j; landings data). Log-means ($\mu_{n,j}$ and $v_{n,j}$) from fisheries-independent and fisheries-dependent simulations, respectively, used model parameter estimates informed by the original data, and σ_n were log-standard deviations used in the survey indices fisheries-dependent and fisheries-independent observation models. The best model was defined as the model with the lowest of this summed PPL. These new simulations-estimated observations for both the fisheries-dependent and fisheries-independent models were then compared with the original data via the above PPL equation to determine the lognormal likelihood of each model. The value of N was chosen as the point at which all model simulations posterior predictive loss value stabilized.

Fig. 2. (Left graphs) Log-quadratic climate-dependent natural mortality (QM) model for estimated ($N_{t,a}$; black line) ± 95% credible interval (CI; grey shaded region) and observed ± 1 standard deviation (black points) survey indices of abundance from 1982 to 2015. (Right graphs) The QM estimated population abundance-at-age ($I_{t,a}$; solid black line) ± 95% CI (dark grey shaded region) compared with the climate-independent (TI) estimated population abundance-at-age ($I_{t,a}$; dotted grey line) ± 95% CI (light grey) from 1982 to 2015.

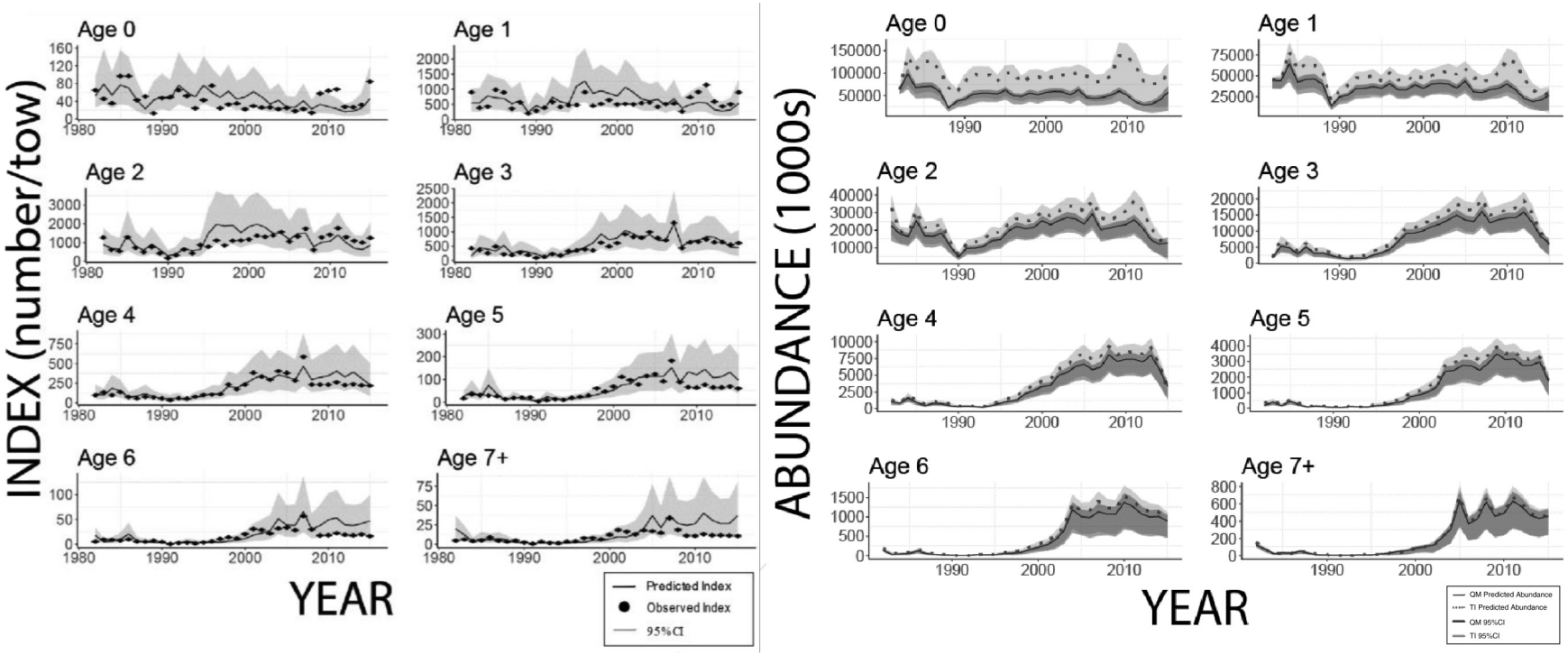

Fig. 3. Two times the spawning stock biomass (SSB) from the log-quadratic climate-dependent natural mortality (QM) model (black solid line) ± 95% credible interval (CI; dark grey shaded region) and two times the SSB from the climate-independent (TI) model (grey dotted line) ± 95% CI (light grey shaded region) for direct comparison with the stock assessment SSB (black dashed line; Terceiro 2016) from 1982 to 2015. The QM and TI models SSB was modeled as 0.5 × $N(t)$, whereas the stock assessment was $N(t)$, so doubling the QM and TI SSB allowed for direct comparison.

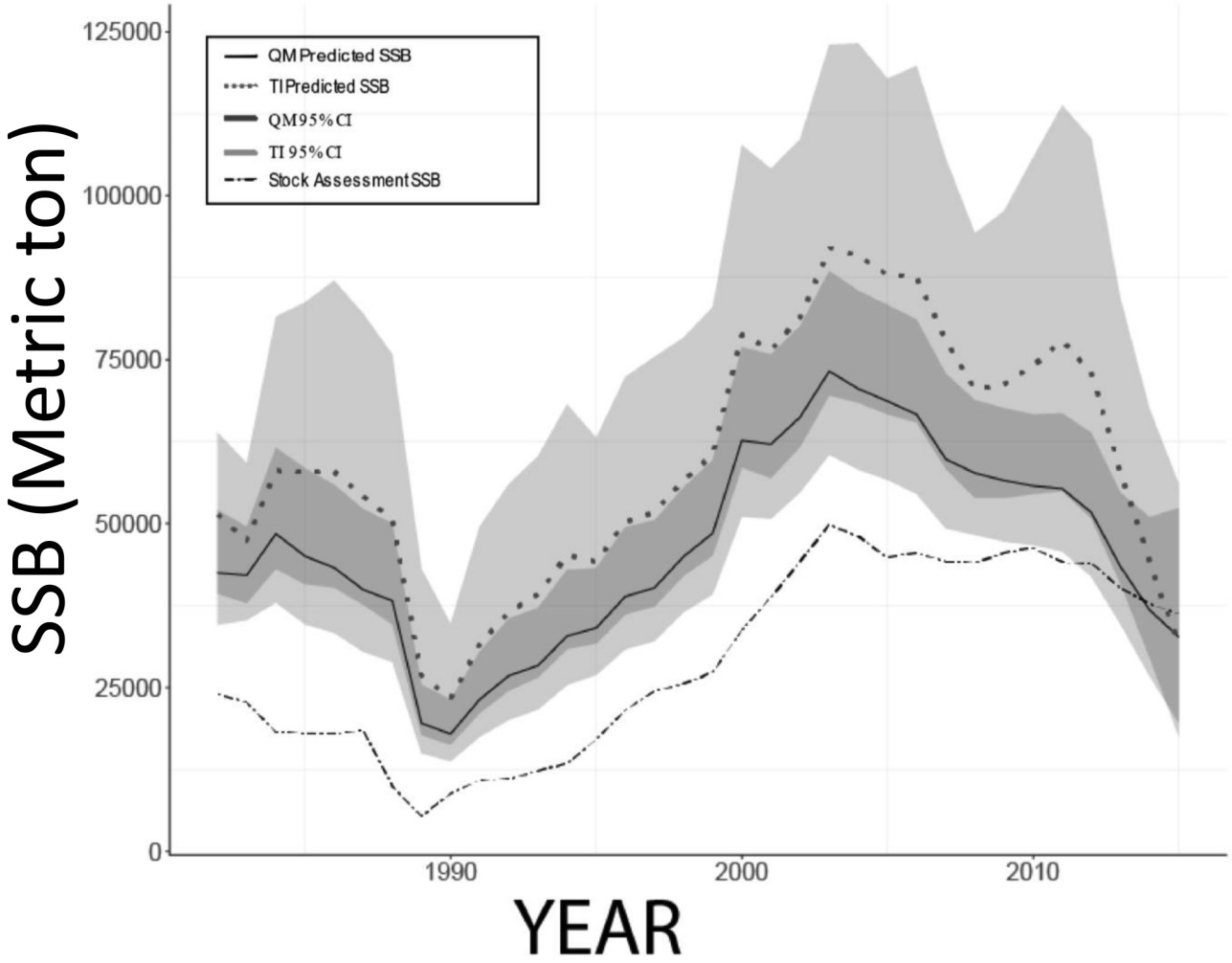

Model performance was also assessed using Mohn's ρ.

$$\rho(\theta) = \frac{\hat{\theta}_{R-r,R-r}}{\hat{\theta}_{R-r,R}} - 1$$

where R is the terminal year of the data series for the full model (here this is 2015), r is the number of years of data removed (peeled) from the full model, $\hat{\theta}_{R-r,R-r}$ is the estimate of a parameter for year $R - r$ from the peel model, and $\hat{\theta}_{R-r,R}$ is the corresponding estimate from the full model (Mohn 1999). A total of seven peels were used for consistency with stock assessment (Terceiro 2013, 2016; Miller and Legault 2017). A smaller absolute value Mohn's $\rho(\theta)$ indicates less retrospective pattern and therefore better model performance. The sign of Mohn's $\rho(\theta)$ indicates trend direction.

Results

Model selection using combined lowest values and ranking for PPL and DIC indicated that the best performing model was the log-quadratic climate-dependent natural mortality (QM) model (Table 3). The age-dependent log-linear climate-dependent natural mortality (AM) model followed as the second-best model. The age-dependent log-quadratic climate-dependent natural mortality + controlling recruitment model (i.e., the NQACR model, which combines age-specific log-quadratic natural mortality with controlling recruitment into one model; Table 1) followed these two models in ranking. Model selection using both PPL and DIC indicated that the log-quadratic relationship was a better fit than ignoring the relationship, despite the small relative effect of GSI. As well, the coefficients on the GSI – natural mortality relationship for each age class in the age-dependent log-quadratic climate-dependent natural mortality (NQA) and AM models were very similar in the age-specific models. Finally, the QM is the simplest model out of the top-ranked models that are within 4 PPL and DIC units. Thus, all of these factors combined led to the selection of the QM model out of all models as the best performing model when considering best performance (lowest value) for both PPL and DIC. It should be emphasized that the climate-independent (TI) model performed worse (higher DIC and PPL value) than all models that included climate-dependent natural mortality, including those models with a combined effect of climate recruitment and climate mortality.

Estimated patterns in abundance-at-age increased for ages 2–7+ from 1990 to 2012 (Fig. 2). Estimated abundances for ages 2–7+ declined in the final 3 years (Fig. 2), and spawning stock biomass

Fig. 4. Estimated natural-mortality-at-age ($M_{a,t}$) for the log-quadratic climate-dependent natural mortality (QM) model (black line) ± 95% credible interval (CI; dark grey shaded region) and the climate-independent (TI) model (dotted line) ± 95% CI (light grey shaded region) from 1982 to 2015.

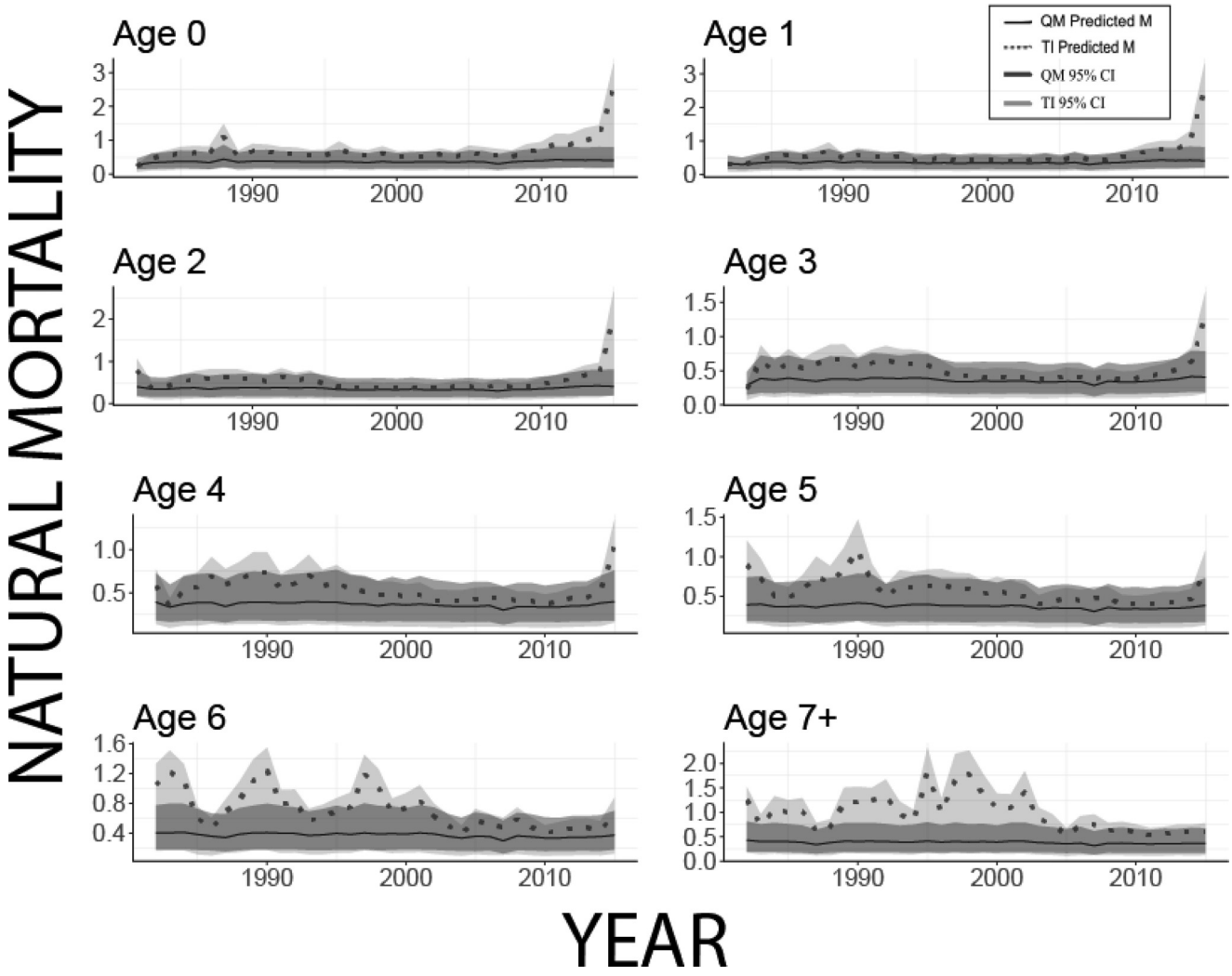

declined from 2004 to 2015 (as estimated by the most recent stock assessment Terceiro 2016; Fig. 3). The QM-model-estimated median index tended to be underestimated for ages 0–2 and overestimated for ages 4–7+ from 2010 to 2015. Before 2010, the QM median index residuals were smaller and more equally distributed than the terminal years. However, the credible intervals (CIs) for all ages captured the indices. These results suggested that there was some process error not captured by the proposed models for the terminal years. The difference between the QM and TI median abundance estimates decreased with age (Fig. 2). The QM model estimated lower abundances-at-age than the TI model for all ages but age 7+ (Fig. 2). The QM model also estimated lower spawning stock biomass than the TI model (Fig. 3).

Model estimations for natural mortality were one of the largest differences between the best-selected models and the climate-independent model, particularly for age classes 0 and 7+ (Fig. 4). Overall, the climate-independent model estimated a higher mean natural mortality across all age classes and years (0.64 ± 0.31 versus 0.37 ± 0.04) and lower mean fishing mortality (0.60 ± 0.44 versus 0.68 ± 0.49) across all age classes and years. Differences between natural mortality model estimations ranged from 0.06 to 2.16 between the TI and QM models for natural mortality estimates (Fig. 4). The largest difference between TI and QM natural mortality estimations was found in age classes 0 to 2 in 2015, a year with a positive GSI value and high fishing mortality. The climate-independent model also estimated average higher abundances for all age classes, with a few exceptions in the final year 2015 and final age class 7+. Natural mortality was much less variable in the QM model that in the TI model. There were also larger differences in median natural mortality for older fish and a smaller difference in median natural mortality for younger fish when comparing the QM model with the TI model. However, CIs do overlap. Fishing pressure was higher for age classes 0 to 5 from 1982 to early 1990s (Terceiro 2013; Terceiro 2016). Fishing rate patterns were similar among all models, although the climate-independent fishing mortality was lower on average for ages 0–6 (Fig. 5). The top five models produced similar overall trends in fishing rate and natural mortality when compared with the QM model (Appendix A). The largest difference was in the size of the CIs for all parameters and the relative estimated abundance for the younger age classes. The index estimations and their associated CIs were nearly identical.

The retrospective analysis revealed a systematic overestimation in the posterior means of fishing mortality and recruitment, and underestimation in the posterior means of spawning stock biomass. Mohn's ρ indicated a difference in model estimates as data were removed when comparing the terminal year estimate in the subset of data with estimates that include data from all years

Fig. 5. Estimated fishing-mortality-at-age ($F_{a,t}$) for the log-quadratic climate-dependent natural mortality (QM) model (black line) ± 95% credible interval (CI; dark grey shaded region) and the climate-independent (TI) model (dotted line) ± 95% CI (light grey shaded region) from 1982 to 2015.

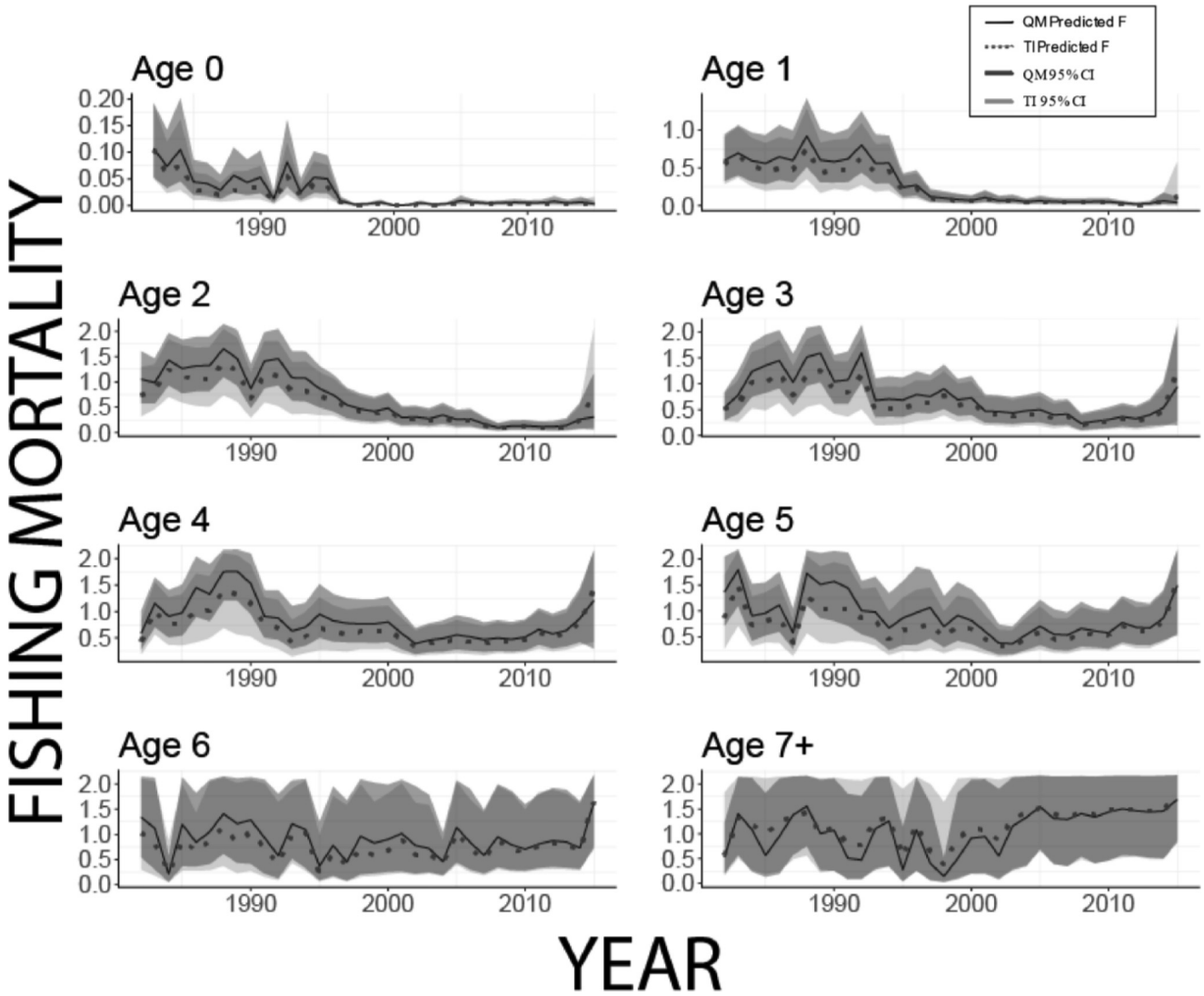

(Fig. 6). Specifically, Mohn's ρ indicates a positive pattern in fishing mortality rate and a negative pattern in spawning stock biomass. The recruitment retrospective pattern varied as data were removed, slightly increasing as data were removed up to 4 years prior and then decreasing as data were further removed. Terminal year recruitment estimates for all peels were between –0.50 and 0.69 less than or greater than the corresponding estimates from the full data set (Mohn's ρ = 0.005). For the QM model, terminal year fishing mortality estimates for all peels ending in 2008–2013 were 0.15–0.25 higher than the corresponding estimates from the full QM data set (Mohn's ρ = 0.15). The difference in terminal year spawning stock biomass estimates for all peels ending in 2008–2013 and the corresponding estimates from the full data set was between –0.56 and 0.08 (Mohn's ρ = 0.08). Mohn's ρ is not related to the magnitude and sign of bias in the terminal year of fish assessments (Hurtado-Ferro et al. 2014). However, it is still undesirable to have estimates that are revised downward or upward consistently with each year of additional data. This retrospective pattern is different from the Terceiro (2016) assessment, although the retrospective patterns are more similar when the Terceiro (2016) model is only run with the NEFSC survey indices like the models presented here (Mark Terceiro, NEFSC, MA, personal communication).

Mean values for the log-quadratic climate-dependent natural mortality equation were $\beta_{0,a}$ = –0.99, $\beta_{1,a}$ = 0.15, and $\beta_{2,a}$ = –1.30. The log-quadratic climate-dependent coefficient and intercept indicated that natural mortality increased as the GSI increases from –2 to 0.26, which indicates a change from a southern Gulf Stream position to an average Gulf Stream position. Natural mortality decreased as GSI increased from 0.26 to 2, indicating that higher temperature waters were extending further into the Northwest Atlantic shelf (Fig. 7).

Finally, the QM model did not appear to follow any obvious stock–recruitment relationship trend (Fig. 8). The QM model estimated lower mean recruitment across time than the TI model (Fig. 8). The QM model estimated higher mean recruitment than Terceiro (2016).

The data in the model informed the ratio of fishing mortality and natural mortality, although the estimation of natural mortality was highly sensitive to the range of the prior on the slope and intercept for the mean function. If natural and fishing mortality were not estimable based upon the catch, trawl, and GSI data,

Fig. 6. Mohn's ρ for 2008–2014 for the log-quadratic climate-dependent natural mortality (QM) model. Mohn's ρ was calculated for fishing mortality, recruitment, and spawning stock biomass (SSB) for the QM model.

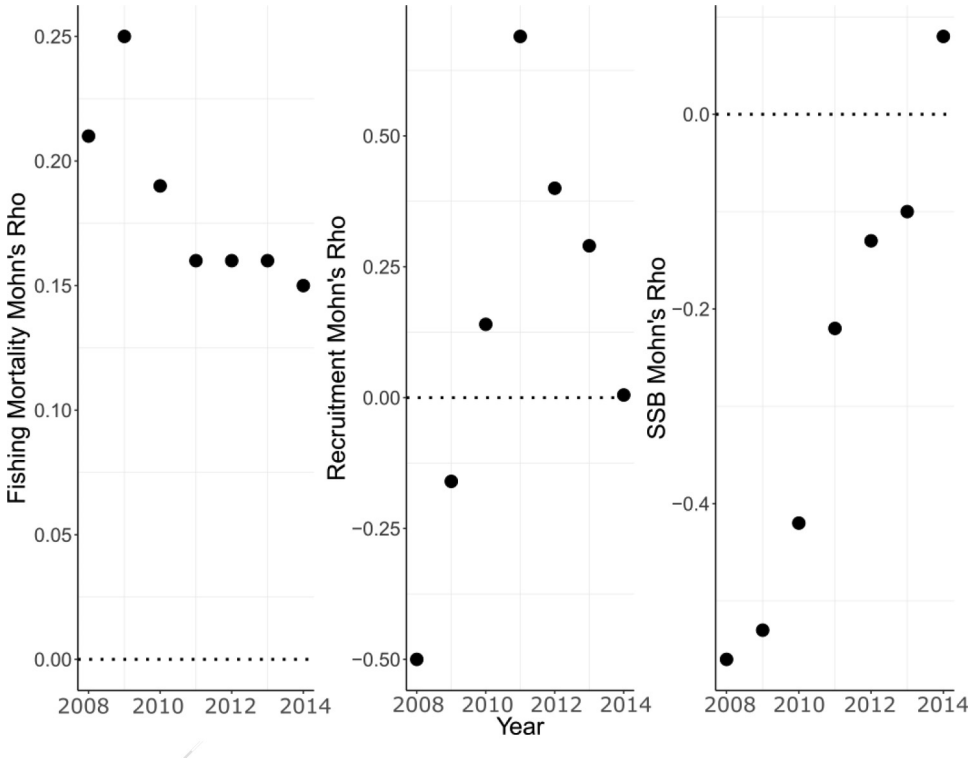

likely the climate-independent model would fare better in model selection. The posterior for β_0 differs from its prior in the selected model and the spread of the β_1 and β_2 posterior is less than their priors, suggesting that some information in the data was able to establish the relationship between GSI and natural mortality (Fig. 9). The GSI – natural mortality relationship allowed some separation of natural and fishing mortality contributions to overall mortality.

Discussion

Testing models with various forms of climate dependency and temporally varying fishing mortality identified a small, yet significant, relative effect of climate dependency alongside fishing mortality in fluctuating summer flounder population abundance. Model results indicated that oceanographic processes, along with varying fishing mortality, played a role in driving the abundance of summer flounder. Climate-dependent natural mortality was more important than climate-dependent recruitment in driving those abundances. The GSI-incorporated models were selected over climate-independent models. By incorporating temporally varying fishing mortality into models with both climate-dependent and climate-independent terms, the selected model indicated that modeling both fluctuating fishing mortality and log-quadratic climate dependency simultaneously better captured past summer flounder abundances than no climate dependency for these tested models.

We note that the log-quadratic climate model was selected over more complicated interaction, recruitment, or age-varying models. This selection suggests that model selection was not simply identifying the model with the most parameters and instead suggests that a parsimonious model was within the range of model complexities considered here. Additionally, model variations that included the log-quadratic natural mortality – GSI relationship and also included recruitment climate dependency were not selected despite having more parameters. The NQA and LM models estimated abundance patterns similar to the QM model, although QM was chosen due to the combined lower PPL and DIC. Interestingly, the difference between the QM and TI abundance estimates decreased with age (Fig. 2). This difference suggests that the position of the Gulf Stream and its related oceanographic conditions influenced natural mortality at younger ages more than older ages. The performance of QM highlights the complexity of the relationship between GSI (and therefore temperature) and natural mortality. An added caveat is that we did not explicitly model net movement, and so climate effects on natural mortality could be aliasing climate effects on the movement of fish outside of the stock area.

Previous work by Terceiro (2013; personal communication) demonstrated that input data and model configuration influence the "optimal" fixed natural mortality value for the assessment model. Such configurations include (*i*) configuration of the age plus group (6+, 7+, 8+, or 10+), (*ii*) configuration of the number of fishing fleets, (*iii*) specification of the estimation of fishery and survey selection, and (*iv*) specification of the explicit stock–recruit function. Therefore, the specification of these configurations is also likely to influence the trend and magnitude of the natural mortality estimate and natural mortality – GSI relationship in the QM model.

There has been a debate in the literature over the importance of fishing mortality versus climate and (or) oceanographic conditions as drivers behind patterns in summer flounder abundance (Nye et al. 2009; Morgan and Mellon 2011; Bell et al. 2015; Morley et al. 2016). In the models presented here, recreational and commercial catches concurrent with various forms of mechanistic climate dependency informed fishing mortality. The difference in prior and posterior distributions suggest that the available data are sufficient to discriminate between stochastic variation in both mortality measures (Fig. 9). Even as fishing mortality after the 1990s decreased below 1 for most age classes, the model containing the relationship between GSI and natural mortality was se-

Fig. 7. The median natural mortality function ($y = \exp(-0.99 + 0.15 \times GSI + -1.30 \times GSI^2)$; dotted line) ± 95% credible interval (CI) for $V_{a,t}$ (without additional variance from natural mortality precision λ_M; grey shaded region) for the log-quadratic climate-dependent natural mortality (QM) model and model predicted posterior distributions for natural mortality $M_{a,t}$ across the Gulf Stream Index (GSI) ± 95% CI (including natural mortality precision λ_M; grey vertical lines) for age 4.

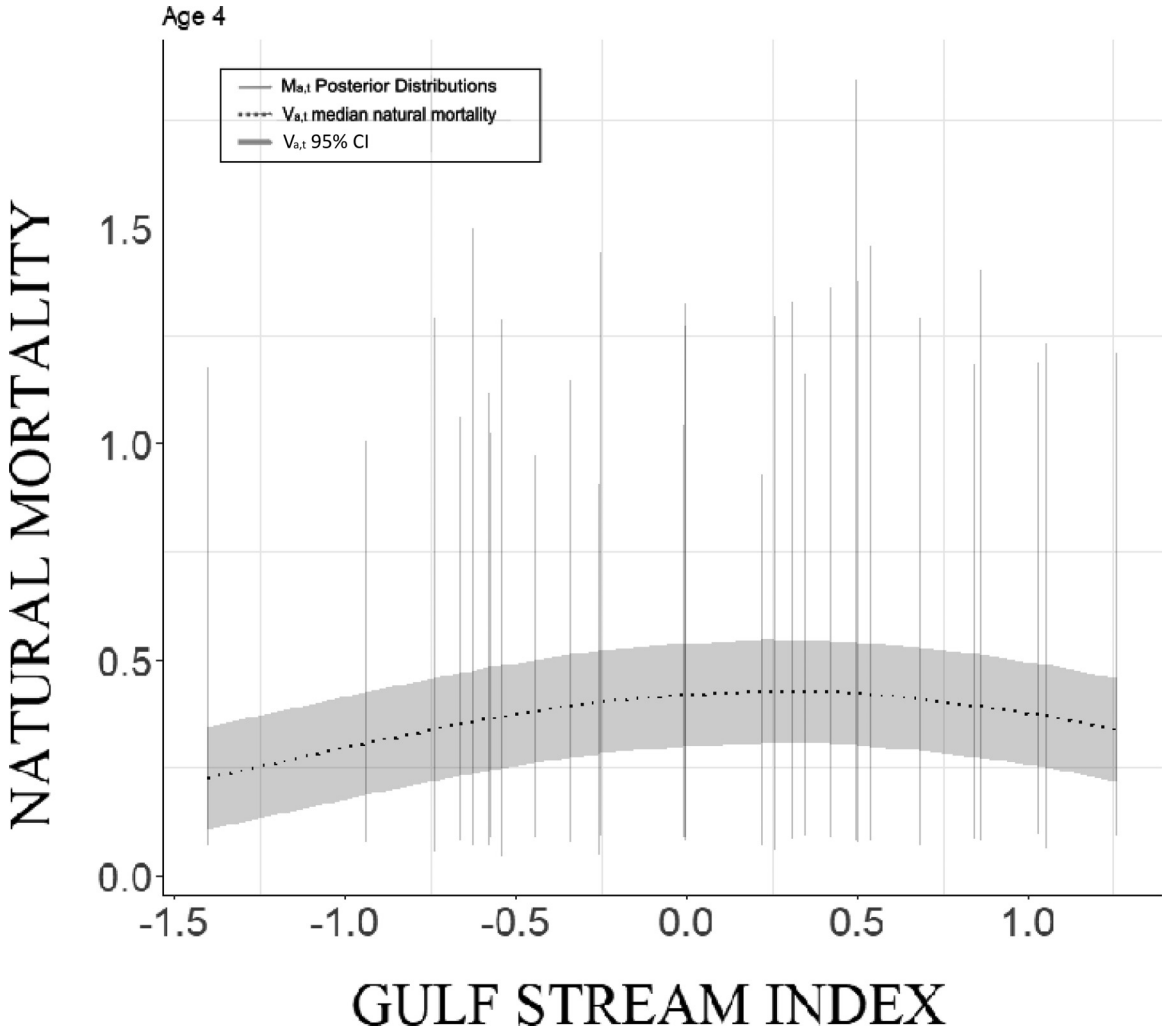

lected. This model selection demonstrated that even when trends in fishing pressure varied over time, oceanographic conditions played a role in summer flounder abundances. Overall, the GSI provided information that improved estimation of natural mortality and subsequently the linked fishing mortality, clarifying the role that both pressures play in past summer flounder abundances.

The GSI is a more integrative representation of the oceanographic conditions on the Northeast US shelf compared with seasonal averages of bottom or surface temperature. It captures the oceanographic properties that the population experiences at moderate spatial and temporal scales and matches the seasonal and spatial scale of the stock assessments in the Northwest Atlantic (Nye et al. 2011; Hallett et al. 2004). While population models represent the emergent properties of the physiology of individual organisms, basin-scale indices such as the GSI represent the emergent properties of the local environment to which individual organisms are responding. The estimated effect of GSI on natural mortality may be small because summer flounder on the Northeast US shelf are at the poleward range limit (and therefore coldest conditions). The log-quadratic nature of the GSI – natural mortality relationship coincides with the life history of summer flounder that prefer warmer temperatures that occur at high GSI. Warm water preferences may also explain the slight decrease in natural mortality as GSI increases from 0.26 to 2. Small increases in temperature bring summer flounder closer to their preferred temperature and therefore optimal survival conditions in this region. We also suggest that the apparent link between natural mortality and the GSI is in part because summer flounder can take advantage of new and warmer habitat further north along the Northwest Atlantic shelf in varying degrees, dependent on mobility (Kleisner et al. 2017). Mobility, ontogenetic migration, lower predator density, higher prey density, and physiological responses are all viable explanations for the dome shape of average natural mortality as GSI increases (Lorenzen 1996). New habitats that older individuals can reach may provide more optimal thermal conditions and less competition for prey items with the rest of the stock, therefore reducing overall natural mortality slightly.

If physiological stress caused the relationship between GSI and natural mortality, we would expect natural mortality to be higher at the GSI extremes. Instead, natural mortality was lower at the GSI extremes, suggesting an ecological mechanism rather than a physiological response to temperature minima and maxima. Previous work demonstrated that as summer duration increases the summer flounder center of biomass moves further north and summer flounder biomass increases (Henderson et al. 2017). These

Fig. 8. Log-quadratic climate-dependent natural mortality (QM) model mean estimated recruitment from 1982 to 2015 (left) and QM model mean recruitment versus mean spawning stock biomass (SSB) (right). The left plot shows recruitment from 1982 to 2015 for the QM model (black solid line) surrounded by the 95% credible interval (CI; dark grey shaded region), for the climate-independent (TI) model (dotted grey line) surrounded by the 95% CI (light grey shaded region), and for Terceiro (2016) stock assessment output (black dashed line). The right plot shows the mean QM model recruitment equation (solid black line), the QM posterior mean estimate for each year (black dots), the QM 10% CI for the mean posterior value (dark grey shaded region), the QM 95% CI for the mean posterior value (medium grey shaded region), and the full posterior predictive distribution QM 95% CI (light grey shaded region) for the log normal distribution.

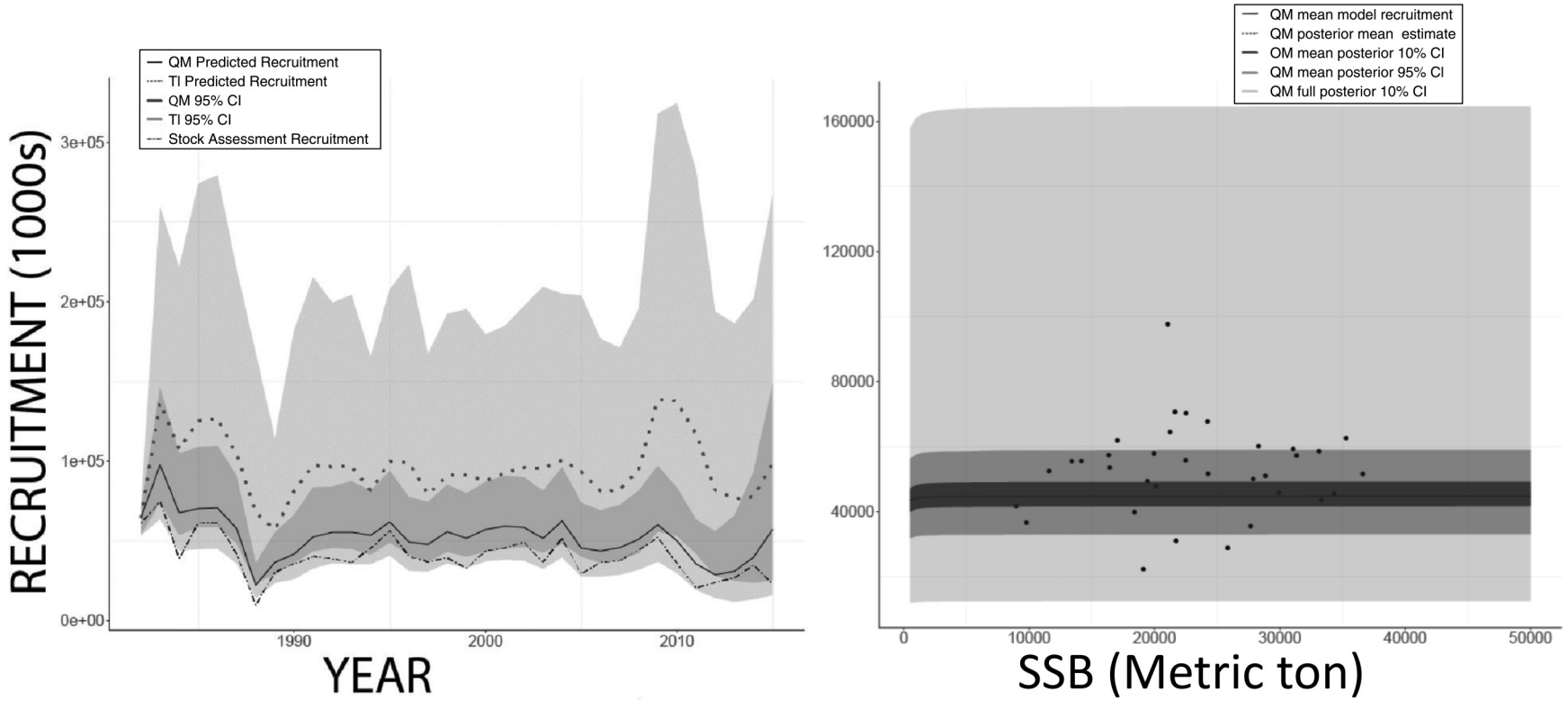

Fig. 9. Prior (white) and posterior (grey) distributions for fishing mortality (F), first polynomial (β_1), second polynomial (β_2), and intercept (β_0) for the climate-dependent natural mortality (QM) model.

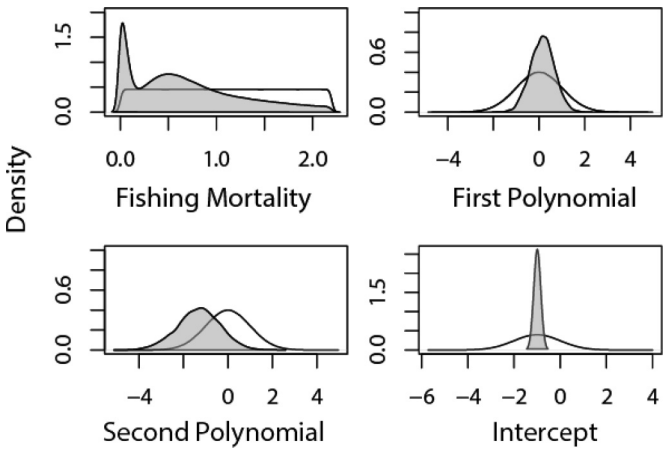

results contrast with previous results observed for the southern New England yellowtail flounder, a flatfish species at the southern end of the species' range in this region, that had reduced recruitment and lower population productivity when GSI was higher (Miller et al. 2016; Xu et al. 2018). However, we have not explicitly modeled density- or climate-dependent processes for the weight-at-age relationship or climate impacts on fecundity (i.e., the offspring per weight relationship) that ultimately impact mortality and recruitment. Weight-at-age and fecundity are important topics for future research on climate linkages.

A notable difference in the output of this model versus the stock assessment output is the spawning stock biomass estimation (Terceiro 2016). The latest stock assessment update indicated a strong increase in spawning stock biomass following the early 1990s, followed by a relatively small decrease from 2003 onward (Terceiro 2016). While the selected model here indicated the same increase in spawning stock biomass up to 2003, the rate of increase was lower. Furthermore, the decrease after 2003 in spawning stock biomass in our selected model is much greater than the Terceiro (2016) stock assessment. Recent stock assessment reports indicated that biomass was overpredicted and fishing mortality underpredicted (Terceiro 2015). Major differences between this study and the stock assessment that may explain differences in spawning stock biomass estimates include (*i*) climate dependency in summer flounder (and the inclusion of natural mortality dependent on GSI), (*ii*) different model structure (e.g., the stock assessment model separated landings and discards, and so has two fleets instead of one), and (*iii*) pooled annual summer flounder fisheries-independent survey in the tested models versus seasonal data in Terceiro (2016). (The pooled rate in this study might lead to alternate conclusions than if the entire fishery was represented in a more detailed manner (Punt et al. 2000*a*, 2000*b*; Maunder and Punt 2004; Berger et al. 2017; Lee et al. 2017). As this was not a full stock assessment, the model structure does not contain seasonal estimates of parameters and, thus, could result in a slightly different spawning stock biomass estimate. However, an exploratory analysis demonstrated that both the fall and spring indices had a similar average and variance with no significant difference between the two data sets (independent *t* test; p value = 0.94). Future extensions of this work should consider a model that looks at seasonal differences in these life history parameter estimates. Including seasonal differences would determine if the climate dependency varies with the inclusion of seasonal information and if this led to any differences between this study and the Terceiro (2016) stock assessment. Finally, the assumed 50:50 sex ratio may need to be considered in future model efforts and will likely impact the spawning stock biomass and recruitment estimation. Female summer flounder are larger than males, and the female-specific fishing mortality rates have increased since 2013 due to minimum retention size regulations (Morson et al. 2015).

While these models suggest environmental drivers of summer flounder abundances alongside fishing mortality, they do not resolve summer flounder spatial structure. Along the east coast of the US, larger and older summer flounder are found in the north, while younger, smaller summer flounder are found in the south (Terceiro 2016; Kleisner et al. 2017). The population was found to be expanding in the northern edge of their range and contracting at the southern edge (Terceiro 2013, 2016), suggesting that this expansion at the northern edge could be a result of expanding age and size structure, not a movement in response to warming waters. Future research could explore these alternative hypotheses using a spatially explicit model that includes spatial variation in recruitment over time (Kristensen et al. 2014; Thorson et al. 2015*a*, 2015*b*).

Future studies should consider the following changes in model structure: (*i*) separate out fishing by type and area, (*ii*) observation precision as age and time variant, (*iii*) temporally correlated natural mortality, (*iv*) a lagged relationship between natural mortality, recruitment, and GSI, and (*v*) other Northwest Atlantic environmental indices that can potentially better represent flatfish dynamics than those found in Xu et al. (2018). Additionally, future studies should consider growth patterns and the total summer flounder range in the Northwest Atlantic and how they relate to fishing pressure and climate. How growth and range relate to fishing pressure and climate will help to resolve if changes in distribution and the size-structure along the eastern seaboard are due to movement and (or) changes in growth and mortality facilitated by climate, fishing effort, or both.

Overall, abundance patterns were best explained by a model that considered log-quadratic climate-dependent natural mortality and varying fishing mortality. However, the specific mechanism causing a shift northward in summer flounder's spatial distribution is still unresolved. This study provides evidence that oceanographic processes and fishing mortality must be considered simultaneously to understand population dynamics in fishes fully. Similar new modeling approaches should be developed to better understand how fishing and climate interact to drive population dynamics in other stocks. Our approach adds to the understanding of the relative roles of climate and fishing on summer flounder population dynamics beyond simple correlation studies, but mechanisms remain elusive. The approach described in this study can be extended into other systems and species to uncover more about the combined role of fishing and climate on other fish populations.

Acknowledgements

We thank Mark Terceiro (NEFSC) for valuable comments, consultations, and providing additional data. We also thank Phil McDowall (SBU) for his consultation in code production and Heather Lynch for her valuable manuscript review comments. We thank Lequan Chi for computing the Joyce's Gulf Stream Index. Finally, we thank the anonymous reviewers for their thorough and thoughtful feedback. This work was supported by Regional Sea Grant award R/MARR14NJ-NY and NOAA Fisheries Sea Grant Population and Ecosystem Dynamics Fellowship. The authors have no substantial competing financial, professional, or personal interests that might have influenced the materials presented in this manuscript.

References

Andres, M. 2016. On the recent destabilization of the Gulf Stream path downstream of Cape Hatteras. Geophys. Res. Lett. **43**(18): 9836–9842. doi:10.1002/2016GL069966.

Azarovitz, T.R. 1981. A brief historical review of the Woods Hole Laboratory trawl survey time series. Can. Spec. Publ. Fish. Aquat. Sci. **58**(62): 67.

Barange, M., Merino, G., Blanchard, J.L., Scholtens, J., Harle, J., Allison, E.H., Allen, J.I., Holt, J., and Jennings, S. 2014. Impacts of climate change on marine ecosystem production in societies dependent on fisheries. Nat. Clim. Change, **4**: 211–216. doi:10.1038/nclimate2119.

Barton, A.D., Greene, C.H., Monger, B.C., and Pershing, A.J. 2003. The Continuous Plankton Recorder survey and the North Atlantic Oscillation: interannual- to multidecadal-scale patterns of phytoplankton variability in the North Atlantic Ocean. Prog. Oceanogr. **58**(2–4): 337–358. doi:10.1016/j.pocean.2003.08.012.

Baudron, A.R., Needle, C.L., and Marshall, C.T. 2011. Implications of a warming North Sea for the growth of haddock *Melanogrammus aeglefinus*. J. Fish Biol. **78**: 1874–1889. doi:10.1111/j.1095-8649.2011.02940.x. PMID:21651538.

Baudron, A.R., Needle, C.L., Rijnsdorp, A.D., and Tara, Marshall, C. 2014. Warming temperatures and smaller body sizes: synchronous changes in growth of North Sea fishes. Global Change Biology, **20**(4): 1023–1031. doi:10.1111/gcb.12514. PMID:24375891.

Belkin, I.M. 2009. Rapid warming of large marine ecosystems. Prog. Oceanogr. **81**(1): 207–213. doi:10.1016/j.pocean.2009.04.011.

Bell, R.J., Richardson, D.E., Hare, J.A., Lynch, P.D., and Fratantoni, P.S. 2015. Disentangling the effects of climate, abundance, and size on the distribution of marine fish: an example based on four stocks from the Northeast US shelf. ICES J. Mar. Sci. **72**(5): 1311–1322. doi:10.1093/icesjms/fsu217.

Berger, A.M., Goethel, D.R., Lynch, P.D., Quinn, T., II, Mormede, S., McKenzie, J., and Dunn, A. 2017. Space oddity: the mission for spatial integration. Can. J. Fish. Aquat. Sci. **74**(11): 1698–1716. doi:10.1139/cjfas-2017-0150.

Blanchard, J.L., Mills, C., Jennings, S., Fox, C.J., Rackham, B.D., Eastwood, P.D., O'Brien, C.M. 2005. Distribution–abundance relationships for North Sea Atlantic cod (*Gadus morhua*): observation versus theory. Can. J. Fish. Aquat. Sci. **62**(9): 2001–2009. doi:10.1139/f05-109.

Brander, K.M. 2007. Global fish production and climate change. Proc. Natl. Acad. Sci. **104**(50): 19709–19714. doi:10.1073/pnas.0702059104. PMID:18077405.

Brander, K. 2010. Impacts of climate change on fisheries. J. Mar. Syst. **79**: 389–402. doi:10.1016/j.jmarsys.2008.12.015.

Broms, K.M., Hooten, M.B., and Fitzpatrick, R.M. 2016. Model selection and assessment for multi-species occupancy models. Ecology, **97**(7): 1759–1770. doi:10.1890/15-1471.1. PMID:27859174.

Brown, R. 2009. Design and field data collection to compare the relative catchabilities of multispecies bottom trawl surveys conducted on the NOAA ship Albatross IV and the FSV Henry B.

Buckley, L.J., Caldarone, E.M., and Lough, R.G. 2004. Optimum temperature and food-limited growth of larval Atlantic cod (*Gadus morhua*) and haddock (*Melanogrammus aeglefinus*) on Georges Bank. Fish. Oceanogr. **13**(2): 134–140. doi:10.1046/j.1365-2419.2003.00278.x.

Burnham, K.P., and Anderson, D.R. 1998. Practical use of the information-theoretic approach. *In* Model selection and inference. Springer, New York. pp. 75–117.

Burns, T.S., Schultz, R., and Brown, B.E. 1983. The commercial catch sampling program in the northeastern United States. Can. Spec. Publ. Fish. Aquat. Sci. 66.

Clark, W.G., St-Pierre, G., and Brown, E.S. 1997. Estimates of halibut abundance from NMFS trawl surveys. International Pacific Halibut Commission Technical Report, 37.

Essington, T.E., Moriarty, P.E., Froehlich, H.E., Hodgson, E.E., Koehn, L.E., Oken, K.L., Siple, M.C., and Stawitz, C.C. 2015. Fishing amplifies forage fish population collapses. Proc. Natl. Acad. Sci. **112**(21): 6648–6652. doi:10.1073/pnas.1422020112. PMID:25848018.

Fry, F.E.J. 1971. The effect of environmental factors on the physiology of fish. Fish Physiol. **6**: 1–98. doi:10.1016/S1546-5098(08)60146-6.

Fuller, E., Brush, E., and Pinsky, M.L. 2015. The persistence of populations facing climate shifts and harvest. Ecosphere, **6**(9): art153. doi:10.1890/ES14-00533.1.

Gelfand, A.E., and Ghosh, S.K. 1998. Model choice: a minimum posterior predictive loss approach. Biometrika, **85**(1): 1–11. doi:10.1093/biomet/85.1.1.

Gelman, A., Carlin, J.B., Stern, H.S., Dunson, D.B., Vehtari, A., and Rubin, D.B. 2014. Bayesian data analysis. Vol. 2. CRC Press, Boca Raton, Fla.

GISTEMP Team. 2018. GISS surface temperature analysis (GISTEMP) [online]. NASA Goddard Institute for Space Studies. Available from https://data.giss.nasa.gov/gistemp/ [accessed 6 March 2018].

Greene, C.H., Meyer-Gutbrod, E., Monger, B.C., McGarry, L.P., Pershing, A.J., Belkin, I.M., Fratantoni, P.S., Mountain, D.G., Pickart, R.S., and Proshutinsky, A. 2013. Remote climate forcing of decadal-scale regime shifts in Northwest Atlantic shelf ecosystems. Limnol. Oceanogr. **58**: 803–816. doi:10.4319/lo.2013.58.3.0803.

Hallett, T., Coulson, T., Pilkington, J., Clutton-Brock, T., Pemberton, J., and Grenfell, B. 2004. Why large-scale climate indices seem to predict ecological processes better than local weather. Nature, **430**: 71–75. doi:10.1038/nature02708. PMID:15229599.

Hansen, J., Ruedy, R., Sato, M., and Lo, K. 2010. Global surface temperature change. Rev. Geophys., **48**: RG4004. doi:10.1029/2010RG000345.

Hare, J.A., Alexander, M.A., Fogarty, M.J., Williams, E.H., and Scott, J.D. 2010. Forecasting the dynamics of a coastal fishery species using a coupled climate–population model. Ecol. Appl. **20**(2): 452–464. doi:10.1890/08-1863.1. PMID:20405799.

Henderson, M.E., Mills, K.E., Thomas, A.C., Pershing, A.J., and Nye, J.A. 2017. Effects of spring onset and summer duration on fish species distribution and biomass along the Northeast United States continental shelf. Rev. Fish Biol. Fish. **27**(2): 411–424. doi:10.1007/s11160-017-9487-9.

Holsman, K.K., Essington, T., Miller, T.J., Koen-Alonso, M., and Stockhausen, W.J. 2012. Comparative analysis of cod and herring production dynamics across 13 northern hemisphere marine ecosystems Mar. Ecol. Prog. Ser., **459**: 231–246. doi:10.3354/meps09765.

Hooten, M.B., and Hobbs, N.T. 2015. A guide to Bayesian model selection for ecologists. Ecol. Monogr. **85**(1): 3–28. doi:10.1890/14-0661.1.

Hurtado-Ferro, F., Szuwalski, C.S., Valero, J.L., Anderson, S.C., Cunningham, C.J., Johnson, K.F., Licandeo, R., et al. 2015. Looking in the rear-view mirror: bias and retrospective patterns in integrated, age-structured stock assessment models. ICES J. Mar. Sci. **72**(1): 99–110. doi:10.1093/icesjms/fsu198.

Iles, T.C., and Beverton, R.J.H. 1998. Stock, recruitment and moderating processes in flatfish. J. Sea Res. **39**(1): 41–55. doi:10.1016/S1385-1101(97)00022-1.

IPCC. 2013. Climate Change 2013: The Physical Science Basis. Contribution of Working Group I to the Fifth Assessment Report of the Intergovernmental Panel on Climate Change. *Edited by* T.F. Stocker, D. Qin, G.-K. Plattner, M. Tignor, S.K. Allen, J. Boschung, A. Nauels, Y. Xia, V. Bex, and P.M. Midgley. Cambridge University Press, Cambridge, United Kingdom and New York, USA. doi:10.1017/CBO9781107415324.

Joyce, T.M., and Zhang, R. 2010. On the path of the Gulf Stream and the Atlantic meridional overturning circulation. J. Clim. **23**(11): 3146–3154. doi:10.1175/2010JCLI3310.1.

Joyce, T.M., Deser, C., and Spall, M.A. 2000. The relation between decadal variability of subtropical mode water and the North Atlantic oscillation. J. Clim. **13**: 2550–2569. doi:10.1175/1520-0442(2000)013<2550:TRBDVO>2.0.CO;2.

King, R. 2012. A review of Bayesian state-space modelling of capture-recapture–recovery data. Interface Focus, **2**(2): 190–204. doi:10.1098/rsfs.2011.0078. PMID:23565333.

Kjesbu, O.S. 1994. Time of start of spawning in Atlantic cod (*Gadus morhua*) females in relation to vitellogenic oocyte diameter, temperature, fish length and condition. J. Fish Biol. **45**(5): 719–735. doi:10.1111/j.1095-8649.1994.tb00939.x.

Kleisner, K.M., Fogarty, M.J., McGee, S., Hare, J.A., Moret, S., Perretti, C.T., and Saba, V.S. 2017. Marine species distribution shifts on the U.S. Northeast Continental Shelf under continued ocean warming. Prog. Oceanogr. **153**: 24–36. doi:10.1016/j.pocean.2017.04.001.

Kristensen, K., Thygesen, U.H., Andersen, K.H., and Beyer, J.E. 2014. Estimating spatio-temporal dynamics of size-structured populations. Can. J. Fish. Aquat. Sci. **71**(2): 326–336. doi:10.1139/cjfas-2013-0151.

Laurel, B.J., Stoner, A.W., and Hurst, T.P. 2007. Density-dependent habitat selection in marine flatfish: the dynamic role of ontogeny and temperature. Mar. Ecol. Prog. Ser. **338**: 183–192. doi:10.3354/meps338183.

Lee, H.-H., Piner, K.R., Maunder, M.N., Taylor, I.G., and Methot, R.D., Jr. 2017. Evaluation of alternative modelling approaches to account for spatial effects due to age-based movement. Can. J. Fish. Aquat. Sci. **74**(11): 1832–1844. doi:10.1139/cjfas-2016-0294.

Lehodey, P., Alheit, J., Barange, M., Baumgartner, T., Beaugrand, G., Drinkwater, K., Fromentin, J.-M., Hare, S.R., Ottersen, G., Perry, R.I., Roy, C., van der Lingen, C.D., and Werner, F. 2006. Climate variability, fish, and fisheries. J. Clim. **19**: 5009–5030. doi:10.1175/JCLI3898.1.

Lorenzen, K. 1996. The relationship between body weight and natural mortality in juvenile and adult fish: a comparison of natural ecosystems and aquaculture. J. Fish Biol. **49**(4): 627–642. doi:10.1111/j.1095-8649.1996.tb00060.x.

Lozier, M.S., Leadbetter, S., Williams, R.G., Roussenov, V., Reed, M.S., and Moore, N.J. 2008. The spatial pattern and mechanisms of heat-content change in the North Atlantic. Science, **319**(5864): 800–803. doi:10.1126/science.1146436. PMID:18174399.

Mann, K.H., and Drinkwater, K.F. 1994. Environmental influences on fish and shellfish production in the Northwest Atlantic. Environ. Rev. **2**(1): 16–32. doi:10.1139/a94-002.

Maunder, M.N., and Punt, A.E. 2004. Standardizing catch and effort data: a review of recent approaches. Fish. Res. **70**(2): 141–159. doi:10.1016/j.fishres.2004.08.002.

Miller, T.J. 2013. A comparison of hierarchical models for relative catch efficiency based on paired-gear data for US Northwest Atlantic fish stocks. Can. J. Fish. Aquat. Sci. **70**(9): 1306–1316. doi:10.1139/cjfas-2013-0136.

Miller, T.J., and Legault, C.M. 2017. Statistical behavior of retrospective patterns and their effects on estimation of stock and harvest status. Fish. Res. **186**: 109–120. doi:10.1016/j.fishres.2016.08.002.

Miller, T.J., Hare, J.A., and Alade, L.A. 2016. A state-space approach to incorporating environmental effects on recruitment in an age-structured assessment model with an application to southern New England yellowtail flounder. Can. J. Fish. Aquat. Sci. **73**(8): 1261–1270. doi:10.1139/cjfas-2015-0339.

Mohn, R. 1999. The retrospective problem in sequential population analysis: An investigation using cod fishery and simulated data. ICES J. Mar. Sci. **56**(4): 473–488. doi:10.1006/jmsc.1999.0481.

Monim, M. 2017. Seasonal and inter-annual variability of Gulf Stream warm core rings from 2000 to 2016. Doctoral dissertation, Master's thesis, University of Massachusetts Dartmouth.

Morgan, M.G., and Mellon, C. 2011. Certainty, uncertainty, and climate change. Clim. Change, **108**(4): 707–721. doi:10.1007/s10584-011-0184-8.

Morley, J.W., Batt, R.D., and Pinsky, M.L. 2016. Marine assemblages respond rapidly to winter climate variability. Global Change Biol. **23**(7): 2590–2601. doi:10.1111/gcb.13578. PMID:27885755.

Morse, W.W. 1981. Reproduction of the summer flounder, *Paralichthys dentatus* (L.). J. Fish Biol. **19**(2): 189–203. doi:10.1111/j.1095-8649.1981.tb05823.x.

Morson, J.M., Bochenek, E.A., Powell, E.N., Hasbrouck, E.C., Gius, J.E., Cotton, C.F., Gerbino, K., and Froehlich, T. 2015. Estimating the sex composition of the summer flounder catch using fishery-independent data. Mar. Coast. Fish. **7**(1): 393–408. doi:10.1080/19425120.2015.1067261.

Mountain, D.G. 2012. Labrador slope water entering the Gulf of Maine — response to the North Atlantic oscillation. Continental Shelf Res. **47**: 150–155. doi:10.1016/j.csr.2012.07.008.

Neill, W.H., Miller, J.M., Van Der Veer, H.W., and Winemiller, K.O. 1994. Ecophysiology of marine fish recruitment: a conceptual framework for understanding interannual variability. Netherlands J. Sea Res. **32**(2): 135–152. doi:10.1016/0077-7579(94)90037-X.

Nye, J.A., Link, J.S., Hare, J.A., and Overholtz, W.J. 2009. Changing spatial distribution of fish stocks in relation to climate and population size on the Northeast United States continental shelf. Mar. Ecol. Prog. Ser. **393**: 111–129. doi:10.3354/meps08220.

Nye, J.A., Joyce, T.M., Kwon, Y.O., and Link, J.S. 2011. Silver hake tracks changes in Northwest Atlantic circulation. Nat. Commun. **2**: 412. doi:10.1038/ncomms1420. PMID:21811241.

Ottersen, G., and Stenseth, N.C. 2001. Atlantic climate governs oceanographic and ecological variability in the Barents Sea. Limnol. Oceanogr. **46**(7): 1774–1780. doi:10.4319/lo.2001.46.7.1774.

Ottersen, G., Planque, B., Belgrano, A., Post, E., Reid, P.C., and Stenseth, N.C. 2001. Ecological effects of the North Atlantic oscillation. Oecologia, **128**(1): 1–14. doi:10.1007/s004420100655. PMID:28547079.

Ottersen, G., Helle, K., and Bogstad, B. 2002. Do abiotic mechanisms determine interannual variability in length-at-age of juvenile Arcto-Norwegian cod? Can. J. Fish. Aquat. Sci. **59**(1): 57–65. doi:10.1139/f01-197.

Parmesan, C. 2006. Ecological and evolutionary responses to recent climate change. Annu. Rev. Ecol. Evol. Syst. **37**: 637–669. doi:10.1146/annurev.ecolsys.37.091305.110100.

Peña-Molino, B., and Joyce, T.M. 2008. Variability in the slope water and its relation to the Gulf Stream path. Geophys. Res. Lett. **35**(3). doi:10.1029/2007GL032183.

Pinsky, M.L., Worm, B., Fogarty, M.J., Sarmiento, J.L., and Levin, S.A. 2013. Marine taxa track local climate velocities. Science, **341**(6151): 1239–1242. doi:10.1126/science.1239352. PMID:24031017.

Planque, B., Fromentin, J.M., Cury, P., Drinkwater, K.F., Jennings, S., Perry, R.I., and Kifani, S. 2010. How does fishing alter marine populations and ecosystems sensitivity to climate? J. Mar. Syst. **79**(3–4): 403–417. doi:10.1016/j.jmarsys.2008.12.018.

Plummer, M. 2003. JAGS: A program for analysis of Bayesian graphical models using Gibbs sampling. *In* Proceedings of the 3rd International Workshop on Distributed Statistical Computing, Vienna, Austria, 22–23 March 2003. 124 (125.10).

Punt, A.E., Walker, T.I., Taylor, B.L., and Pribac, F. 2000*a*. Standardization of catch and effort data in a spatially-structured shark fishery. Fish. Res. **45**: 129–145. doi:10.1016/S0165-7836(99)00106-X.

Punt, A.E., Pribac, F., Walker, T.I., Taylor, B.L., and Prince, J.D. 2000*b*. Stock assessment of school shark, *Galeorhinus galeus*, based on a spatially-explicit population dynamics model. Mar. Freshw. Res. **51**: 205–220. doi:10.1071/MF99124.

R Core Team. 2017. R: a language and environment for statistical computing [computer program]. R Foundation for Statistical Computing, Vienna, Austria. Available from https://www.R-project.org/.

Richardson, D.E., Palmer, M.C., and Smith, B.E. 2014. The influence of forage fish abundance on the aggregation of Gulf of Maine Atlantic cod (*Gadus morhua*) and their catchability in the fishery. Can. J. Fish. Aquat. Sci. **71**(9): 1349–1362. doi:10.1139/cjfas-2013-0489.

Saba, V.S., Griffies, S.M., Anderson, W.G., Winton, M., Alexander, M.A., Delworth, T.L., Hare, J.A., et al. 2016. Enhanced warming of the Northwest Atlantic Ocean under climate change. J. Geophys. Res. Oceans, **121**(1): 118–132. doi:10.1002/2015JC011346.

Simpson, S.D., Jennings, S., Johnson, M.P., Blanchard, J.L., Schön, P.J., Sims, D.W., and Genner, M.J. 2011. Continental shelf-wide response of a fish assemblage to rapid warming of the sea. Curr. Biol. **21**(18): 1565–1570. doi:10.1016/j.cub.2011.08.016. PMID:21924906.

Solberg, T.S., and Tilseth, S. 1987. Variations in growth pattern among yolk-sac larvae of cod (*Gadus morhua* L.) due to differences in rearing temperature and light regime. Sarsia, **72**: 347–349. doi:10.1080/00364827.1987.10419734.

Somerton, D. 1996. Estimating trawl catchability. Alaska Fisheries Science Center Quarterly Report, April–May–June, pp. 1–3.

Su, Y.S., and Yajima, M. 2012. R2jags: A Package for Running JAGS from R. R package version 0.03-08 [computer program]. Available from http://CRAN.R-project.org/package=R2jags.

Szuwalski, C.S., Vert-Pre, K.A., Punt, A.E., Branch, T.A., and Hilborn, R. 2015. Examining common assumptions about recruitment: a meta-analysis of recruitment dynamics for worldwide marine fisheries. Fish Fish. **16**(4): 633–648. doi:10.1111/faf.12083.

Taylor, C.C., Bigelow, H.B., and Graham, H.W. 1957. Climate trends and the distribution of marine animals in New England. Fish. Bull. **57**: 293–345.

Terceiro, M. 2013. Stock assessment of summer flounder for 2013. U.S. Department of Commerce, National Oceanic and Atmospheric Administration, National Marine Fisheries Service, Northeast Fisheries Science Center.

Terceiro, M. 2015. Stock assessment update of summer flounder for 2015. U.S. Dept. Commer., Northeast Fish. Sci. Cent. Ref. Doc. 15-13.

Terceiro, M. 2016. Stock assessment of summer flounder for 2016. U.S. Department of Commerce, National Oceanic and Atmospheric Administration, National Marine Fisheries Service, Northeast Fisheries Science Center.

Thorson, J.T., Monnahan, C.C., and Cope, J.M. 2015*a*. The potential impact of time-variation in vital rates on fisheries management targets for marine fishes. Fish. Res. **169**: 8–17. doi:10.1016/j.fishres.2015.04.007.

Thorson, J.T., Ianelli, J.N., Munch, S.B., Ono, K., and Spencer, P.D. 2015*b*. Spatial delay-difference models for estimating spatiotemporal variation in juvenile production and population abundance. Can. J. Fish. Aquat. Sci. **72**(12): 1897–1915. doi:10.1139/cjfas-2014-0543.

Thorson, J.T., Rindorf, A., Gao, J., Hanselman, D.H., and Winker, H. 2016. Density-dependent changes in effective area occupied for sea-bottom-associated marine fishes. Proc. R. Soc. B Biol. Sci. **283**(1840): 20161853. doi:10.1098/rspb.2016.1853. PMID:27708153.

Thorson, J.T., Ianelli, J.N., and Kotwicki, S. 2017. The relative influence of temperature and size-structure on fish distribution shifts: a case-study on Walleye pollock in the Bering Sea. Fish Fish. **18**(6): 1073–1084. doi:10.1111/faf.12225.

Townsend, D.W., Rebuck, N.D., Thomas, M.A., Karp-Boss, L., and Gettings, R.M. 2010. A changing nutrient regime in the Gulf of Maine. Continental Shelf Research, **30**(7): 820–832. doi:10.1016/j.csr.2010.01.019.

Van Der Kraak, G., and Pankhurst, N.W. 1996. Temperature effects on the reproductive performance of fish. *In* Global warming: implications for freshwater and marine fish. *Edited by* C.M. Wood and D.G. McDonald. Cambridge University Press, Cambridge, U.K. pp. 159–176.

Vert-pre, K.A., Amoroso, R.O., Jensen, O.P., and Hilborn, R. 2013. Frequency and intensity of productivity regime shifts in marine fish stocks. Proc. Natl. Acad. Sci. **110**(5): 1779–1784. doi:10.1073/pnas.1214879110. PMID:23322735.

Xu, H., Kim, H.M., Nye, J.A., and Hameed, S. 2015. Impacts of the North Atlantic Oscillation on sea surface temperature on the Northeast US Continental Shelf. Continental Shelf Research, **105**: 60–66. doi:10.1016/j.csr.2015.06.005.

Xu, H., Miller, T.J., Hameed, S., Alade, L.A., and Nye, J.A. 2018. Evaluating the utility of the Gulf Stream Index for predicting recruitment of Southern New England-Mid Atlantic yellowtail flounder. Fish. Oceanogr. **27**(1): 85–95. doi:10.1111/fog.12236.

Appendix A

Comparison of spawning stock biomass and natural mortality estimates for the top five performing models

The greatest difference in the top five performing models was in the precision of posterior distributions. In general, models with a much worse (higher) PPL and DIC ranking had much larger CIs for most parameter posterior distributions. Overall, the inclusion of a GSI effect reduced CIs. However, the CIs were often larger for models with GSI effects included in both the natural mortality and recruitment terms than the models with a single GSI effect. The top five models produced similar overall trends in fishing rate and natural mortality when compared with best performing model (QM). The largest difference was in the size of the CIs for all parameters and the relative estimated abundance for the younger age classes. Natural mortality varied more at older ages (Fig. A1). Natural mortality CIs were largest for the log-quadratic climate-dependent natural mortality + controlling recruitment (QMCR) model out of the top five models. The DIC and PPL values were greater than 4 units apart for this model, indicative of its significantly poorer performance. The overall spawning stock biomass trends were similar among top performing models as well (Fig. A2). Finally, the annual relative median value and overall CI range differences between top models was greatest for the younger age classes (Fig. A3). Again, the overall predicted trend in median abundance was similar for top performing models. The index predictions and their associated CIs were nearly identical.

Fig. A1. Predicted natural-mortality-at-age ($M_{t,a}$) for the top five best performing models and their associated ±95% credible interval (CI) from 1982 to 2015. Top five models are log-quadratic climate-dependent natural mortality (QM) model ± 95% CI, age-dependent log-linear natural mortality (AM), the age-dependent log-quadratic natural mortality + controlling recruitment (NQACR), log-quadratic natural mortality (NQA), and log-quadratic natural mortality + controlling recruitment (QMCR). The credible intervals for each model from darkest (smallest) grey to lightest (widest) grey are QM, AM, NQA, NQACR, QMCR.

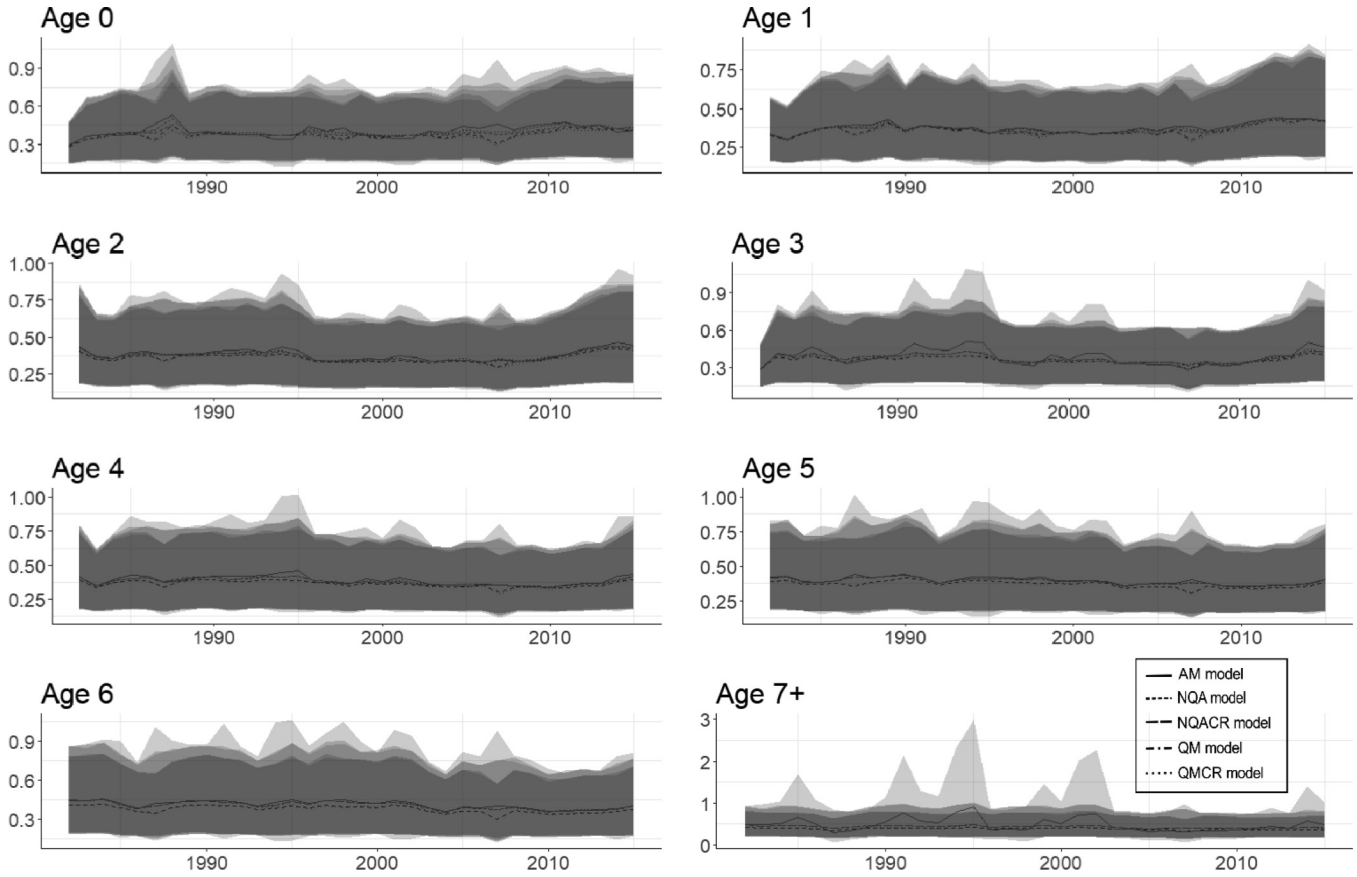

Fig. A2. Two times the spawning stock biomass (SSB) from the log-quadratic climate-dependent natural mortality (QM) model ± 95% credible interval (CI), two times the SSB from the age-dependent log-linear natural mortality (AM) model ± 95% CI, two times the SSB from the age-dependent log-quadratic natural mortality + controlling recruitment (NQACR) model ± 95% CI, two times the SSB from the log-quadratic natural mortality (NQA) model ± 95% CI, and two times the SSB from the log-quadratic natural mortality + controlling recruitment (QMCR) model ± 95% CI for direct comparison with the stock assessment SSB (Terceiro 2016) from 1982 to 2015. The SSBs from this study were modeled as $0.5 \times N(t)$, whereas the stock assessment was $N(t)$, so doubling the SSB from this study allowed for direct comparison.

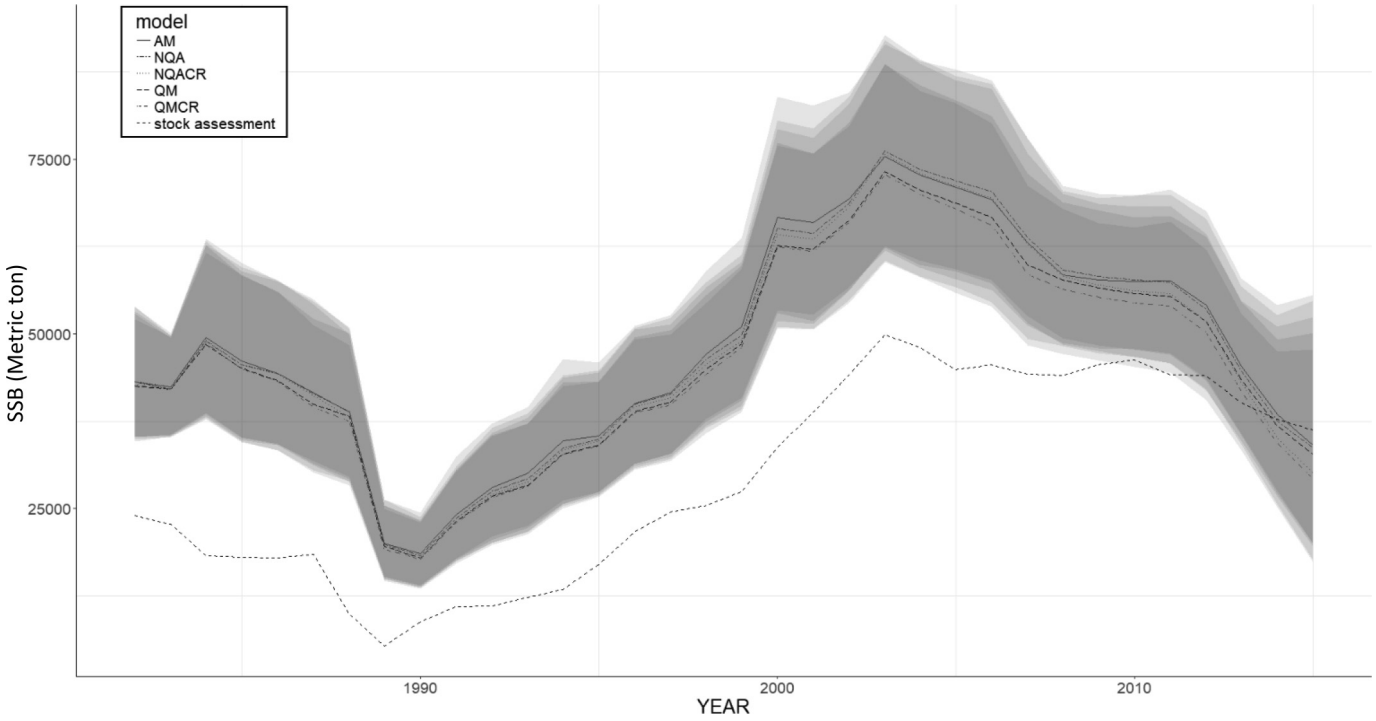

Fig. A3. Predicted population abundance-at-age ($I_{t,a}$) ± 95% credible interval (CI) from 1982 to 2015 for the top five best performing models. Top five models are log-quadratic climate-dependent natural mortality (QM) model ± 95% CI, age-dependent log-linear natural mortality (AM), the age-dependent log-quadratic natural mortality + controlling recruitment (NQACR), log-quadratic natural mortality (NQA), and log-quadratic natural mortality + controlling recruitment (QMCR). The credible intervals for each model from darkest (smallest) grey to lightest (widest) grey are QM, AM, NQA, NQACR, QMCR.